

Differential interferon- α subtype immune signatures suppress SARS-CoV-2 infection

Schuhenn J. ^{1*}, Meister T.L. ^{2*}, Todt D. ^{2,3}, Bracht T. ^{4,5}, Schork K. ^{4,6}, Billaud J.-N. ⁷, Elsner C. ¹, Heinen N², Karakoes Z. ¹, Haid S. ⁸, Kumar S. ⁹, Brunotte L. ^{9, 10}, Eisenacher M. ^{4,6}, Chen J. ¹¹, Yuan Z ¹¹, Pietschmann T. ^{8, 12, 13}, Wiegmann B. ¹⁴, Beckert H. ¹⁵, Taube C. ¹⁵, Le-Trilling VTK. ¹, Trilling M. ¹, Krawczyk A. ^{1,16}, Ludwig S. ^{9, 10}, Sitek B. ^{4,5}, Steinmann E. ², Dittmer U. ¹, Sutter K. ^{1*#} and Pfaender S. ^{2*#}

Affiliation:

¹University Hospital Essen, University Duisburg-Essen, Institute for Virology, Essen, Germany

²Ruhr-University-Bochum, Molecular and Medical Virology, Bochum, Germany

³European Virus Bioinformatics Center (EVBC), Jena, Germany

⁴Ruhr-University-Bochum, Medizinisches Proteom-Center, Bochum, Germany

⁵University Hospital Knappschaftskrankenhaus Bochum, Department of Anesthesia, Intensive Care Medicine and Pain Therapy, Bochum, Germany

⁶Ruhr-University Bochum, Center for Protein Diagnostics (PRODI), Medical Proteome Analysis, Bochum, Germany

⁷Qiagen Digital Insights, Redwood City, California, United States

⁸Twincore, Department of Experimental Virology, Hannover, Germany

⁹Westfaelische Wilhelms-University, Institute of Virology Muenster, Münster, Germany

¹⁰Interdisciplinary Centre for Clinical Research, University of Muenster, Muenster, Germany

¹¹MOE & NHC Key Laboratory of Medical Molecular Virology, School of Basic Medical Sciences, Shanghai Medical College, Fudan University, Shanghai, China.

¹²Cluster of Excellence RESIST (EXC 2155), Hannover Medical School, Carl-Neuberg-Straße 1, 30625 Hannover, Germany

¹³German Center for Infection Research (DZIF), Partner Site Hannover-Braunschweig, 30625 Hannover, Germany

¹⁴Hannover Medical School, Department for Cardiothoracic, Transplantation and Vascular Surgery, Hannover, Germany

¹⁵University Medical Center Essen - Ruhrlandklinik, Department of Pulmonary Medicine, Experimental Pneumology, Essen, Germany

¹⁶University Hospital Essen, Department of Infectious Diseases, West German Centre of Infectious Diseases, Essen, Germany

* Equally contributing author

Correspondence: Kathrin.sutter@uni-due.de; Stephanie.pfaender@rub.de

1 **Summary**

2 Type I interferons (IFN-I) exert pleiotropic biological effects during viral infections, balancing
3 virus control versus immune-mediated pathologies and have been successfully employed for
4 the treatment of viral diseases. Humans express twelve IFN-alpha (α) subtypes, which activate
5 downstream signalling cascades and result in distinct patterns of immune responses and
6 differential antiviral responses. Inborn errors in type I IFN immunity and the presence of anti-
7 IFN autoantibodies account for very severe courses of COVID-19, therefore, early
8 administration of type I IFNs may be protective against life-threatening disease. Here we
9 comprehensively analysed the antiviral activity of all IFN α subtypes against SARS-CoV-2 to
10 identify the underlying immune signatures and explore their therapeutic potential. Prophylaxis
11 of primary human airway epithelial cells (hAEC) with different IFN α subtypes during SARS-
12 CoV-2 infection uncovered distinct functional classes with high, intermediate and low antiviral
13 IFNs. In particular IFN α 5 showed superior antiviral activity against SARS-CoV-2 infection.
14 Dose-dependency studies further displayed additive effects upon co-administered with the
15 broad antiviral drug remdesivir in cell culture. Transcriptomics of IFN-treated hAEC revealed
16 different transcriptional signatures, uncovering distinct, intersecting and prototypical genes of
17 individual IFN α subtypes. Global proteomic analyses systematically assessed the abundance of
18 specific antiviral key effector molecules which are involved in type I IFN signalling pathways,
19 negative regulation of viral processes and immune effector processes for the potent antiviral
20 IFN α 5. Taken together, our data provide a systemic, multi-modular definition of antiviral host
21 responses mediated by defined type I IFNs. This knowledge shall support the development of
22 novel therapeutic approaches against SARS-CoV-2.

23

24 **Keywords:** Type I IFN, IFN α subtypes, SARS-CoV-2, COVID-19, antiviral treatment,
25 remdesivir, therapy, ISG

26 **Main**

27 Without the capacity to produce or recognize interferons (IFN), mammalian hosts rapidly
28 succumb in case of viral infections. Accordingly, humans with loss-of-function mutations in
29 the IFN signalling pathway even fail to control attenuated viruses. Therefore., IFNs are
30 indispensable mediators of the first immediate intrinsic cellular defences against invading
31 pathogens, such as viruses. So far, three different types of IFNs, types I, II and III, have been
32 identified and classified based on their genetic, structural, and functional characteristics as well
33 as receptor usages¹⁻³. Type I IFNs are among the first line of antiviral defence due to the
34 ubiquitous expression of the surface receptor IFNAR consisting of two subunits IFNAR1 and
35 IFNAR2. In humans, the type I IFN family comprises IFN β , IFN ϵ , IFN κ , IFN ω and twelve
36 IFN α subtypes. The latter code for the distinct human IFN α proteins: IFN α 1, -2, -4, -5, -6, -7, -
37 8, -10, -14, -16, -17 and -21, encoded by 14 nonallelic genes including one pseudogene and two
38 genes that encode identical proteins (IFN α 13 and IFN α 1). The overall identity of the IFN α
39 proteins ranges from 75 to 99% amino acid sequence identity^{1,4}. Despite their binding to the
40 same cellular receptor, their antiviral and antiproliferative potencies differ considerably⁵⁻¹⁰. As
41 a general event in terms of signal transduction, IFN α subtypes engage the IFNAR1/2 receptor
42 and initiate a signal transduction cascade resulting in the phosphorylation of receptor-associated
43 janus tyrosine kinases culminating in downstream signalling events including the activation of
44 IFN-stimulated gene factor 3 (ISGF3) consisting of phosphorylated STAT1 and STAT2 and
45 the IFN regulatory factor 9. ISGF3 binding to the IFN-stimulated response elements (ISRE), in
46 promotor regions of various genes, initiates the transcriptional activation of a large number of
47 IFN-stimulated genes (ISGs), which elicit direct antiviral, anti-proliferative and
48 immunoregulatory properties¹¹. It is largely elusive, why different IFN α proteins exhibit
49 distinct effector functions. Different receptor affinities and/or interaction interfaces within the
50 IFNAR have been discussed which may account for the observed variability in the biological
51 activity^{12,13}. Furthermore, the dose, the cell type, the timing and the present cytokine milieu

52 might further affect the IFN effector response¹⁴. In the absence of specific antiviral drugs,
53 treatment of patients with type I IFNs is often considered as first therapeutic response, given its
54 successful clinical application against viral infections^{15,16}. Recently, type III IFNs (IFN-lambda,
55 IFNλ) received significant attention and are currently explored in clinical trials¹⁷. IFNλ binds
56 to the type III IFN receptor, which is preferentially expressed on epithelial cells and certain
57 myeloid cells¹⁸, resulting in restricted cell signalling and compartmentalized activity.
58 Especially at epithelial surface barriers, IFNλ mount an effective local innate immune response,
59 by conferring viral control and inducing immunity without generating systemic activation of
60 the immune system which could trigger pathologic inflammatory responses. Signal transduction
61 cascades of type I and type III IFNs are considered to be rather similar resulting in overlapping
62 ISG signatures, however, type I IFN signalling leads to a more rapid induction and decline of
63 ISG expression¹⁹.

64 The outbreak of novel viruses, as exemplified by the recent emergence of *Severe Acute*
65 *Respiratory Syndrome Coronavirus-2* (SARS-CoV-2), causing the disease COVID-19 has
66 emphasised the urgent need for fast and effective therapeutic strategies. Indeed, type I IFN
67 treatment is currently explored as emergency treatment against COVID-19 in various clinical
68 trials²⁰⁻²², and it was already shown that SARS-CoV-2 is sensitive to type I IFNs²³ and ISGs²⁴.
69 Given their large genome size, CoVs have evolved a variety of strategies circumventing the
70 host innate immune reaction, including evasion strategies targeting type I IFN signalling^{23,25-27}.
71 Along those lines, recent studies showed significantly decreased interferon activity in COVID-
72 19 patients who developed more severe disease²⁸, highlighting the importance of IFN in
73 controlling viral infection. Against viruses, pegylated IFNα2 is approved and frequently
74 administered in clinical settings. However, common side effects include the occurrence of flu-
75 like symptoms, haematological toxicity, elevated transaminases, nausea, fatigue, and
76 psychiatric sequelae, which often result from systemic activation of the immune system²⁹.
77 Given the described distinct biological properties of IFNα subtypes, we comprehensively

78 studied their antiviral effect against SARS-CoV-2 in comparison to another respiratory virus
79 (influenza A virus), and we aimed to explore SARS-CoV-2-specific immune signatures that
80 could contribute to an efficient viral clearance. Accordingly, the aim of this study was two-fold:
81 I) to identify underlying immune-signatures crucial for controlling SARS-CoV-2 infection and
82 II) to explore the therapeutic potential of IFN α subtypes in SARS-CoV-2 infection.

83

84 **Results**

85 *IFN α subtypes differentially inhibit SARS-CoV-2*

86 In order to determine the antiviral potencies of the twelve different IFN α subtypes against
87 SARS-CoV-2, we pre-treated VeroE6 cells with two doses (1000 units per mL (U/mL) and 100
88 U/mL). We included IFN λ 3 (1000 ng/mL and 100 ng/mL), since its potent antiviral activity
89 against SARS-CoV-2 and other respiratory pathogens has been documented^{30,31}. Following
90 treatment for 16 hours, cells were subsequently infected with SARS-CoV-2 and viral replication
91 was quantified by determining infectious viruses (TCID₅₀/mL) and genome amplification.
92 Interestingly, we observed a differential antiviral pattern for the individual subtypes, with
93 IFN α 5, α 4, α 14 and IFN λ 3 exhibiting the strongest antiviral effects with up to 10⁵ fold reduction
94 in viral titres (Figure 1A and Extended Data Figure 1A). Immunofluorescence analysis of
95 VeroE6 cells pre-treated with IFN α 5, IFN α 7 and IFN α 16 confirmed their different antiviral
96 activities against SARS-CoV-2 (Figure 1B). To determine the inhibitory concentration 50
97 (IC₅₀), we performed dose-response analyses covering concentrations from 19 to 80,000 U/mL
98 for the pre-treatment. SARS-CoV-2 replication was assessed by quantification of viral titres
99 (TCID₅₀/mL) and viral antigens applying a previously described in-cell ELISA³² (Table 1 and
100 Extended Data 1B-D). Corroborating previous results, a striking clustering of the antiviral
101 subtypes according to their antiviral potency was observed, which allowed their separation into
102 classes of low (IC₅₀ > 5000 U/mL), intermediate (IC₅₀: 2000-5000 U/mL) and high (IC₅₀: < 2000
103 U/mL) antiviral activities against SARS-CoV-2 (Fig. 1C-F, Extended Data 1B-D, Table 1).

104 Since VeroE6 cells are derived from African green monkey, expressing the non-human primate
105 instead of human IFN receptor and also lack the capacity to produce IFN-I in a natural feed-
106 forward loop³³, we further analysed genuine target cells of SARS-CoV-2. We utilized well-
107 differentiated primary human airway epithelial cells (hAEC), which closely resemble the *in*
108 *vivo* physiology of the respiratory system, and differentiate into various cells types, resulting in
109 ciliary movement and production of mucus^{34,35}. After IFN pre-treatment and subsequent
110 infection with SARS-CoV-2, apical washes were monitored concerning viral replication
111 kinetics at 33°C³⁶. Cells were lysed at 72 h post infection (p.i.) and viral progeny (Fig. 1G, H)
112 as well as viral *M* and *N* gene expression (Extended Data 1 E-J) were determined. Again, a
113 distinct antiviral pattern became evident (Figure 1G) defining IFN clusters of high (IFN α 5, -4,
114 -14, - IFN λ 3), moderate (IFN α 17, -2, -7, -21) and low antiviral activities (FN α 10, -16, -6, -1)
115 (Fig. 1H and Extended Data 1 G, J). Prototypical ISG expression patterns, as analysed by qRT-
116 PCR, revealed subtype-specific gene expression signatures (Extended Data Figure 2A-E. In
117 order to address if the observed antiviral activities were SARS-CoV-2-specific, we additionally
118 tested influenza A virus (IAV/PR8) in hAECs. Interestingly, pre-treatment of hAECs with the
119 IFN-subtypes revealed differences compared to SARS-CoV-2. In general, antiviral responses
120 could be clustered into strong for α 2, -4, -5, -8, -14 and IFN λ 3 (Fig. 1I) and weak antiviral
121 activities for IFN α 1, -6, -7, -10, -16, -17 and 21 (Fig. 1J). Amongst the strong antiviral
122 responses, we observed additional transient differences at 48 h p.i., with IFN α 2, -4, -5 and -14
123 being slightly superior to IFN α 8 and - λ 3 (Fig. 1I). These results clearly demonstrate that
124 different IFN α subtypes mediate distinct biological and temporal activities.

125

126 *IFN subtype-specific gene expression signatures*

127 Since we observed clear differences in the biological activities of different IFN α subtypes
128 against SARS-CoV-2, we next aimed to identify their underlying immune signatures and
129 mechanisms. To this end, primary hAECs were pre-treated with the respective IFNs and 16 h

130 post stimulation cellular RNA was sequenced on an Illumina NovaSeq 6000 and differentially
131 expressed genes were sent to Ingenuity Pathway Analysis (IPA; Qiagen) for biological analysis.
132 In order to investigate cellular responses following viral infection, we included SARS-CoV-2-
133 infected hAECs (18 h p.i.) in our analysis. Global transcriptomic analysis revealed unique
134 differentially expressed genes (DEGs), both up- and downregulated upon IFN-treatment ^{37,38}
135 for each IFN (Extended Data Figure 3A) compared to mock-treated cells. Similar to the
136 observed antiviral effects, a general clustering was apparent which showed similar expression
137 patterns for low to intermediate antiviral subtypes (IFN α 1, -6, -7, -16, -10, -21) and intermediate
138 to high antiviral subtypes (IFN α 2, -17, -14, -4, -5, - λ 3). Interestingly, we observed a clear
139 difference in the numbers of significantly up- and down-regulated genes after treatment with
140 IFN α subtypes compared to mock-treated cells, which positively correlated with antiviral
141 activity (Extended Data Figure 3B). Gene ontology (GO) pathway analysis revealed higher
142 expression of genes mostly involved in antiviral immune response amongst the medium and
143 high antiviral subtypes, as well as pathways which can be associated with protein localization,
144 translation, oxidative phosphorylation, RNA metabolism, ER stress, signalling pathways and
145 lymphocyte activation (Figure 2A). Strikingly, different IFN α subtypes displayed unique GO
146 patterns with IFN α 17, in contrast to other subtypes, regulating genes involved in translation,
147 whereas the treatment with IFN α 5 resulted in the strongest regulation of genes associated to
148 signalling pathways and lymphocyte activation among all IFNs (Figure 2A). We next focussed
149 on genes associated with antiviral responses (Figure 2B). A separation based on antiviral
150 activity could be discerned with weak antiviral IFN α subtypes (IFN α 1, -6, -16, -10) exhibiting
151 comparatively lower expression values of specific ISGs, whereas medium to strong antiviral
152 IFN α subtypes induced higher expression (Figure 2B). We observed two clusters that differed
153 between low and intermediate to high IFN subtypes, with ISG15, IFI27, MX1 and others
154 showing generally lower expression values in the low antiviral IFN subtypes. Even more
155 pronounced were expression changes of IFIT2, IFIT1 and MX2 and others which resulted in a

156 down-regulation for the low- and an upregulation for the intermediate to high antiviral IFN
157 subtypes. As we aimed at identifying immune signatures that correlate with the antiviral activity
158 against SARS-CoV-2 infection, we next evaluated DEGs with respect to distinct, intersecting
159 and common genes amongst and between subtypes (Extended Data Figure 4A). We identified
160 several differentially expressed genes for each subtype, with IFN α 5 expressing most unique
161 genes (1018 DEGs), followed by IFN λ 3 (670 DEGs) (Figure 2C, Extended Data Figure 4B)).
162 A comparison between high, medium and low antiviral subtypes revealed that 19 genes were
163 commonly differentially expressed amongst all subtypes including *Mx1* and *OAS2* (Figure 2D).
164 The most striking differences could be observed for *MX1* and *OAS2*, which expression levels
165 clearly separated high, intermediate and low antiviral IFN subtypes (Figure 2D). Interestingly,
166 42 genes were differentially regulated in the high antiviral group including *RNaseL* and genes
167 associated with regulation of transcription, signal transduction and metabolic processes (Figure
168 2E), as well as long non-coding RNAs. In conclusion, we could clearly demonstrate IFN
169 subtype-specific immune signatures that could contribute to the observed differences in
170 antiviral activity.

171

172 *Proteomic analysis highlights key cellular factors*

173 Our transcriptomic analysis revealed IFN α subtype-specific distinct, intersecting and common
174 expression patterns of DEGs that most likely contribute to the differential biological activity
175 against SARS-CoV-2. To further uncover relevant cellular effector proteins for the antiviral
176 activity against SARS-CoV-2, we additionally performed proteomic analysis on hAECs pre-
177 treated with IFNs. Since we had observed the strongest antiviral activity for IFN α 5 and IFN λ 3
178 we decided to further investigate their specific proteomic profile in direct comparison with
179 IFN α 7, which exhibited a moderate antiviral effect, and IFN α 16, displaying a weak effect
180 against SARS-CoV-2 infection, in order to identify key antiviral pathways, crucial in
181 controlling coronavirus infection. To this end, primary hAECs were pre-treated with selected

182 IFNs for 16 h. In addition to the early time point (t=0 h), where we aim to identify key cellular
183 factors that are expressed before viral infection, we included a late time point, 72 h post
184 treatment both in the presence (t=72 h [CoV-2]) or absence of viral infection (t=72 h [mock]),
185 to investigate potential antiviral mechanisms and potential intervention by viral effectors
186 (Extended Data Figure 5A). Principal component analysis (PCA) revealed a clustering
187 according to donor and/or infection and time points (Extended data Figure 5B-D, Extended
188 Data Table 2). In addition to host cell proteins, various viral peptides were identified, which
189 correlate to viral titres depending on the respective donor (Extended Data Table 3, Extended
190 Data Figure 5E). For all donors, no SARS-CoV-2 peptides could be detected following
191 treatment with IFN α 5 and IFN λ 3. Pre-treatment of cells with IFN subtypes resulted in up- or
192 down-regulation of a variety of proteins compared to untreated hAECs, depending on the IFN
193 stimulation (Extended Data Figure 6A-C). In order to perform statistical analysis, we
194 considered proteins that were measured in minimum three of four donors, however on/off
195 analysis (defined as full absence of a protein in one group of a pairwise comparison) revealed
196 additional proteins which might be of interest (Extended Data Figure 6D-F, Extended Data
197 Table 4). GO analysis of proteins differentially abundant between untreated and IFN-treated
198 samples at each time point (untreated vs IFN) identified enrichment of antiviral immune
199 responses for all IFNs, except IFN α 16 (Figure 3A, Extended Data Figure 7A). For IFN α 16,
200 only proteins associated with lymphocyte regulation were induced, which likely do not
201 contribute to SARS-CoV-2 restriction in cell culture but may be very important *in vivo*. At 72
202 h pathways belonging to proteolysis, metabolism and protein localization were additionally
203 enriched after treatment with IFN α 5 and λ 3. The most prominent upregulated proteins,
204 associated with IFN signalling (STAT1, MX1, ISG15, ISG20, IFI35, and others) were found to
205 be on-off regulated and present only upon treatment with IFN α 5, α 7 and λ 3. Additional ISGs
206 including IFIT3, OAS2, and IFITM3 were on-off regulated after 72 h and CoV-2 infection
207 except for IFN α 16-treatment (Figure 3B, Extended Data Figure 7B). Interestingly, the

208 comparison of samples in the presence or absence of SARS-CoV-2 (Mock vs CoV-2) showed
209 a striking trend towards downregulation of proteins upon CoV-2 infection. Enrichment of
210 biological processes associated with complement activation and O-glycan processing (Figure
211 3C) highlighted various complement factors (e.g. CFB, C4B and C3) as well as various mucines
212 (e.g. Muc1, Muc16) by SARS-CoV-2, independent of IFN-treatment and resulting viral titres
213 (Figure 3D, Extended Data Figure 7C, E, Extended Data Table 5). In contrast, the strongest
214 biological effects on antiviral immune responses after treatment with IFN α 5 and - λ 3, e.g. IFN
215 signalling as well as antigen presentation, NF- κ B signalling or lymphocyte regulation were not
216 affected by viral infection. Interestingly, proteins belonging to other pathways e.g. antigen
217 presentation by MHC class I or proteolysis, seemed to be less abundantly represented under
218 viral infection in the IFN α 5 treated samples, a phenomenon which was not as prominent after
219 treatment with IFN λ 3 (Figure 3E, Extended Data Figure 7D). STRING analysis (Figure 3F)
220 highlighted the presence of antiviral key effector molecules (e.g. ISG20, ISG15, IFI44L, IFIT2,
221 IFIT3, IFI35, PML, SP100), which are involved in type I IFN signalling pathways, negative
222 regulation of viral processes and immune effector processes amongst the most potent antiviral
223 IFNs. In conclusion, we identified a variety of antiviral cellular effector molecules that correlate
224 with antiviral activity and controlling coronavirus infection

225

226 *Therapeutic potential of IFN α subtypes*

227 Currently, there are only a few approved specific antiviral drugs (e.g. monoclonal
228 antibodies)^{39,40} for the treatment of COVID-19, which severely limit treatment options during
229 severe clinical courses. Remdesivir, a nucleotide-analogous RNA dependent RNA Polymerase
230 (RdRP) inhibitor originally developed as antiviral against Ebola virus, received an emergency
231 use-approval against COVID-19 and has been employed in the clinics. Unfortunately, due to
232 lack of evidence for recovery of critically ill patients, it is no longer recommended by the World
233 Health Organization (WHO) as single treatment for COVID-19⁴¹). Therefore, alternative

234 therapeutic approaches such as combination therapies are urgently needed. As we have
235 observed the strongest antiviral effect in this study for IFN α 5 we explored its therapeutic
236 potential in comparison and in combination with remdesivir. In regard to patients viewed as an
237 entity, prophylactic treatment with IFNs is no clinical option. Nevertheless, a treatment initiated
238 following diagnosis can still ‘prophylactically’ condition and protect cells in the body against
239 later infection events. To monitor the kinetics of the antiviral activity of IFN α subtypes, we
240 treated cells either before infection (‘pre-’) or up to 8 h post infection (‘post-’) and studied the
241 antiviral activity by determining viral titres as TCID₅₀/mL and viral antigens by ic ELISA
242 (Figure 4A, B). As expected, the strongest reduction in viral titres was observed upon pre-
243 treatment with IFN α 5 as cells become alerted towards an antiviral state and antiviral effectors
244 can be transcribed or even translated prior to viral infection (Figure 4B). Intriguingly, even after
245 viral infection was established, treatment with IFN α 5 was able to significantly reduce viral titres
246 (Figure 4B), which was also observed with the antiviral drug remdesivir (Extended Data Figure
247 8A). Given the clear antiviral but incomplete inhibitory effect of both treatment modalities, we
248 next studied a potential beneficial effect of IFN α 5 when co-administered with remdesivir (see
249 Figure 4A for a schema). To this end, we analysed the antiviral effect upon pre-treatment as
250 well as post-treatment of an established infection. To quantify the interaction between the two
251 antiviral drugs, the observed combination response was compared to the expected effect using
252 the Loewe additivity model, with δ -scores above 10 indicating synergistic effects. Combination
253 therapies in VeroE6 cells revealed an additive antiviral activity, with over 90 % viral inhibition
254 upon pre-treatment in the highest concentrations of both drugs tested and a Loewe synergistic
255 score of 8.504 (Figure 4C, D) without any effect on cytotoxicity (Extended Data Figure 8B).
256 Similarly, post-treatment resulted in a dose-dependent, additive viral inhibition with over 70 %
257 (Figure 4E, F). To confirm these findings, we analysed selected combinations of IFN α 5 with
258 remdesivir post-infection in hAEC. For this we combined low doses (0.313 μ M remdesivir,
259 0.2444 U/mL IFN α 5), medium doses (0.63 μ M remdesivir, 15.625 U/mL IFN α 5) and high

260 doses (2.5 μ M remdesivir, 1.953 U/mL IFN α 5), and observed in all combinations an additive
261 therapeutic effect when co-administered 8 h post infection (Figure 3G-I). Taken together, we
262 provide evidence that co-administration of direct antiviral drugs together with potent IFN α
263 subtypes clearly impaired viral replication and might provide an alternative therapeutic
264 approach.

265

266 **Discussion**

267 Type I interferons serve as one of the first lines of defence and are induced almost immediately
268 upon viral encounters. Type I IFN foster intrinsic immunity, stimulate innate immunity, and
269 recruit and orchestrate adaptive immunity. They can modulate the immune system in several
270 ways, by exerting a wide range of biological activities including antiviral, antiproliferative,
271 immunomodulatory and regulatory activities. Importantly, impaired type I IFN activity are
272 correlated with severe courses of COVID-19, highlighting their clinical importance⁴².
273 Accordingly, defectiveness to type I IFNs significantly contributes to disease severity and
274 genetic polymorphisms decreasing IFN-I production are associated with more severe cases of
275 COVID-19⁴³⁻⁴⁵. Furthermore, pegylated IFN α 2a therapy in patients with inborn errors of type
276 I IFN immunity prevented severe COVID-19 disease⁴⁶. In addition to the impaired type I IFN
277 response triggered by SARS-CoV-2, recent studies have demonstrated the development of
278 autoantibodies that can neutralize type I IFNs^{44,47}. To evade the antiviral effects of type I IFNs,
279 viruses have evolved various strategies to suppress IFN induction. SARS-CoV-2 codes for
280 several proteins that have been implicated in type I IFN antagonism, thereby compromising
281 host responses and favouring viral replication⁴⁸. Thus, early administration of IFN-I might be
282 an effective treatment option for COVID-19 patients. The IFN-I family consists of multiple
283 IFN α subtypes, which are highly conserved, and they all signal through the same ubiquitously
284 expressed IFNAR1/2. Activation of various downstream signalling cascades implicates that the
285 IFN α subtypes share some overlapping functions, but also possess unique properties. Upon pre-
286 treatment of cells with twelve distinct IFN α subtypes, we observed cluster-specific antiviral
287 patterns which were distinct between different viruses. These differential antiviral functions
288 cannot be explained solely by the binding affinity to both receptor subunits as IFN α 5 and IFN α 4
289 exhibit a median affinity to IFNAR1 and IFNAR2 in the range of 0.94-3 μ M and 2.1-3.8 nM,
290 respectively¹². Furthermore, the increased gene induction did not correlate with binding affinity
291 to IFNAR1 or 2, as those IFNs with the highest binding affinity to IFNAR2 (IFN α 10, 17, 6, 14,

292 7) did not induce significantly higher numbers of differentially expressed genes. In IFN-treated
293 gut biopsies of chronically HIV-infected patients, the numbers of induced genes by different
294 type I IFNs (IFN α 1, α 2, α 5, α 8, α 14 and β) were not associated with binding affinity or ISRE
295 activation⁴⁹. Importantly, it has been shown that the different type I IFNs induced a specific
296 pattern of genes, which are involved in various biological processes⁴⁹. We observed distinct
297 antiviral patterns, that could be clearly clustered into high, intermediate and low antiviral effects
298 against SARS-CoV-2. Interestingly, we identified 19 genes that were common between all
299 groups, indicative of a basal IFN response. On top of that basal response, we identified several
300 genes that were distinct-, intersecting- or commonly differentially regulated between the high
301 and/or medium group. Our dataset enabled us to identify expression patterns that can be
302 correlated with antiviral activity against SARS-CoV-2. Foremost, antiviral immune responses
303 were significantly dysregulated in the moderate and high antiviral groups. Nevertheless, several
304 biological processes e.g. such associated with protein localization, translation or ER stress,
305 displayed variable induction patterns depending on the IFN α subtype. Proteomic analysis
306 confirmed expression of IFN effector molecules in high and moderate antiviral subtypes. We
307 mostly identified factors involved in type I IFN signalling pathways, negative regulation of
308 viral processes and immune effector processes. These results clearly demonstrate unique and
309 overarching properties of different IFN α subtypes. Another group recently reported that
310 saturated concentrations (1000pg/mL) of IFN α subtypes against HIV-1 *in vitro* induced similar
311 levels of 25 canonical ISGs⁵⁰. The authors concluded from these 25 ISGs that the overall
312 difference between all subtypes is only quantitatively, but not qualitatively, implying that the
313 transcription of 25 genes is fully sufficient to describe the whole interferome⁵¹. We similarly
314 observe a clear difference in the magnitude of differential regulated genes, that likely
315 contributes to the observed antiviral patterns. Nevertheless, as demonstrated with IAV, these
316 patterns do affect virus replication to a different extent, indicating that individual IFN α subtypes
317 might have discriminative clinical effects. Due to its known antiviral activity and its clinical

318 administration in chronic viral infections, type I IFNs, specifically IFN α 2 or IFN β , were already
319 used in a variety of different clinical trials in patients with mild or severe COVID-19. During
320 SARS-CoV-2 infection, two phases can be observed: 1) an early phase with weak IFN α / β
321 production and limited antiviral responses and 2) an excessive inflammatory immune response
322 which can give rise to cytokine storms or acute respiratory distress syndrome. Therefore, a
323 potential beneficial effect of IFN treatment must occur early during infection to not exacerbate
324 hyperinflammation. Early subcutaneous administration of IFN β in combination with
325 lopinavir/ritonavir and ribavirin in patients with mild to moderate COVID-19 led to a
326 significant reduction of symptoms, shortening the duration of viral shedding and hospital stay²².
327 Pulmonary administration of type I IFNs might reduce systemic side effects, while increasing
328 type I IFN concentrations in the infected epithelial cells. Inhaled or nebulized IFN α 2b with
329 arbidol or IFN β -1b showed faster recovery from SARS-CoV-2 infection and decreased levels
330 of inflammatory cytokines^{20,21}. Furthermore, prophylactic intranasal application of IFN α 2a/b in
331 health care workers in China completely prevented new SARS-CoV-2 infections⁵². A recent
332 report from SARS-CoV-2 infection in golden hamsters demonstrated a systemic inflammation
333 in distal organs like brain or intestine⁵³. They hypothesized that virus-derived molecular
334 patterns and not infectious SARS-CoV-2 were disseminated to the periphery leading to
335 systemic inflammation and increased IFN signatures. These observations might further
336 highlight the need to apply type I IFNs via intranasal route or inhalation, as the IFN response
337 in the periphery is already highly stimulated and a systemic administration would not further
338 increase the antiviral host immune response. We clearly demonstrated the additive benefit of
339 combining treatment of type I IFN with a direct acting antiviral, e.g. remdesivir. Taken together,
340 most of the data so far support the administration of type I IFN early during infection to curb
341 viral infection and lessen disease severity. Next to involvement of various cellular pathways,
342 both on transcriptomic as well as proteomic level, we identified novel signatures in primary
343 hAEC after infection with SARS-CoV-2. Strikingly, despite reduced viral replication in the

344 presence of highly antiviral IFN α subtypes, infection with SARS-CoV-2 resulted in a
345 downregulation of O-glycan processing. Mucus plays a vital role in protecting the respiratory
346 tract from various factors, and serves as first line of defence against invading pathogens. Goblet
347 cells secrete soluble mucus which major components are heavily O-glycosylated mucin
348 glycoproteins⁵⁴. Inflammatory conditions result in an increase of soluble and transmembrane
349 mucins, and alteration of their glycosylation to boost mucosal defence^{55,56}. Therefore, it is
350 striking that we observed a consistent downregulation of various mucins upon SARS-CoV-2
351 infection. Some recent studies have highlighted the highest level of expression of ACE2 and
352 TMPRSS2, entry factors utilized by SARS-CoV-2, in the nasal goblet and ciliated cells in
353 healthy individuals, cells which are also associated with high MUC1 and MUC5A expression
354 levels^{57,58}. Therefore, it is likely that these cells represent the initial infection route for the virus.
355 It is tempting to speculate that virus infection of these cells triggers mucin downregulation in
356 order to impede cellular defence mechanisms. Interestingly, a significant proportion of COVID-
357 19 patients represents with dry cough, indicating that downregulation of mucins could
358 contribute to this clinical characteristic. In contrast, a recent study has described elevated
359 MUC1 and MUC5AC protein levels in airway mucus of critical ill COVID-19 patients⁵⁹.
360 However, the authors speculated that elevated mucin levels could originate from detached and
361 disrupted epithelial cells. It will be interesting to further analyze the role of mucins and their
362 glycans during COVID-19 pathogenesis and study the influence of viral replication on mucin
363 expression. In conclusion, in this study we provide a global characterization of the antiviral
364 response of different IFN α subtypes on various levels and uncovered immune signatures which
365 are able to significantly reduce SARS-CoV-2 infection as well as identify novel features after
366 virus infection of primary cell types. Our study contributes to an enhanced understanding of the
367 molecular landscape controlling SARS-CoV-2 infection and could thereby pave the way
368 towards novel therapeutic approaches upon identification of key cellular pathways and factors
369 involved in SARS-CoV-2 infection.

370 **Tables**

371 Table 1: IC₅₀ values of IFN α subtypes on VeroE6 cells obtained from endpoint dilution assay.

IFN α subtype	IC ₅₀ [U/mL]
IFN α 4	56.91
IFN α 14	70.73
IFN α 5	79.73
IFN α 8	327.0
IFN α 2	1026
IFN α 7	2431
IFN α 21	4944
IFN α 16	>5000
IFN α 1	>5000
IFN α 17	>5000
IFN α 6	>5000
IFN α 10	>5000

372

373 **References**

374

- 375 1 Hardy, M. P., Owczarek, C. M., Jermiin, L. S., Ejdeback, M. & Hertzog, P. J.
376 Characterization of the type I interferon locus and identification of novel genes.
377 *Genomics* **84**, 331-345, doi:10.1016/j.ygeno.2004.03.003 (2004).
- 378 2 Mesev, E. V., LeDesma, R. A. & Ploss, A. Decoding type I and III interferon signalling
379 during viral infection. *Nat Microbiol* **4**, 914-924, doi:10.1038/s41564-019-0421-x
380 (2019).
- 381 3 Platanias, L. C. Mechanisms of type-I- and type-II-interferon-mediated signalling. *Nat
382 Rev Immunol* **5**, 375-386 (2005).
- 383 4 Wittling, M. C., Cahalan, S. R., Levenson, E. A. & Rabin, R. L. Shared and Unique
384 Features of Human Interferon-Beta and Interferon-Alpha Subtypes. *Front Immunol* **11**,
385 605673, doi:10.3389/fimmu.2020.605673 (2020).
- 386 5 Chen, J. *et al.* Functional Comparison of Interferon-alpha Subtypes Reveals Potent
387 Hepatitis B Virus Suppression by a Concerted Action of Interferon-alpha and
388 Interferon-gamma Signaling. *Hepatology* **73**, 486-502, doi:10.1002/hep.31282 (2021).
- 389 6 Dickow, J. *et al.* Diverse Immunomodulatory Effects of Individual IFNalpha Subtypes
390 on Virus-Specific CD8(+) T Cell Responses. *Front Immunol* **10**, 2255,
391 doi:10.3389/fimmu.2019.02255 (2019).
- 392 7 Lavender, K. J. *et al.* Interferon Alpha Subtype-Specific Suppression of HIV-1 Infection
393 In Vivo. *J Virol* **90**, 6001-6013, doi:10.1128/JVI.00451-16 (2016).
- 394 8 Harper, M. S. *et al.* Interferon-alpha Subtypes in an Ex Vivo Model of Acute HIV-1
395 Infection: Expression, Potency and Effector Mechanisms. *PLoS pathogens* **11**,
396 e1005254, doi:10.1371/journal.ppat.1005254 (2015).
- 397 9 Gibbert, K., Schlaak, J., Yang, D. & Dittmer, U. IFN-alpha subtypes: distinct biological
398 activities in anti-viral therapy. *British journal of pharmacology* **168**, 1048-1058,
399 doi:10.1111/bph.12010 (2013).
- 400 10 Song, J. *et al.* Different antiviral effects of IFNalpha subtypes in a mouse model of HBV
401 infection. *Sci Rep* **7**, 334, doi:10.1038/s41598-017-00469-1 (2017).

- 402 11 Schoggins, J. W. A diverse range of gene products are effectors of the type I interferon
403 antiviral response. *Nature* **472**, 481-485 (2011).
- 404 12 Lavoie, T. B. *et al.* Binding and activity of all human alpha interferon subtypes. *Cytokine* **56**, 282-289, doi:10.1016/j.cyto.2011.07.019 (2011).
- 405 13 Jaks, E., Gavutis, M., Uze, G., Martal, J. & Piehler, J. Differential receptor subunit
406 affinities of type I interferons govern differential signal activation. *J Mol Biol* **366**, 525-
407 539 (2007).
- 408 14 Tomasello, E., Pollet, E., Vu Manh, T. P., Uze, G. & Dalod, M. Harnessing Mechanistic
409 Knowledge on Beneficial Versus deleterious IFN-I Effects to Design Innovative
410 Immunotherapies Targeting Cytokine Activity to Specific Cell Types. *Frontiers in*
411 *immunology* **5**, 526, doi:10.3389/fimmu.2014.00526 (2014).
- 412 15 Perrillo, R. Benefits and risks of interferon therapy for hepatitis B. *Hepatology* **49**,
413 S103-111, doi:10.1002/hep.22956 (2009).
- 414 16 Tan, G., Song, H., Xu, F. & Cheng, G. When Hepatitis B Virus Meets Interferons. *Front*
415 *Microbiol* **9**, 1611, doi:10.3389/fmicb.2018.01611 (2018).
- 416 17 Chan, H. L. Y. *et al.* Peginterferon lambda for the treatment of HBeAg-positive chronic
417 hepatitis B: A randomized phase 2b study (LIRA-B). *J Hepatol* **64**, 1011-1019,
418 doi:10.1016/j.jhep.2015.12.018 (2016).
- 419 18 Kotenko, S. V., Rivera, A., Parker, D. & Durbin, J. E. Type III IFNs: Beyond antiviral
420 protection. *Semin Immunol* **43**, 101303, doi:10.1016/j.smim.2019.101303 (2019).
- 421 19 Lazear, H. M., Schoggins, J. W. & Diamond, M. S. Shared and Distinct Functions of
422 Type I and Type III Interferons. *Immunity* **50**, 907-923,
423 doi:10.1016/j.jimmuni.2019.03.025 (2019).
- 424 20 Monk, P. D. *et al.* Safety and efficacy of inhaled nebulised interferon beta-1a (SNG001)
425 for treatment of SARS-CoV-2 infection: a randomised, double-blind, placebo-
426 controlled, phase 2 trial. *Lancet Respir Med* **9**, 196-206, doi:10.1016/S2213-
427 2600(20)30511-7 (2021).
- 428 21 Zhou, Q. *et al.* Interferon-alpha2b Treatment for COVID-19 Is Associated with
429 Improvements in Lung Abnormalities. *Viruses* **13**, doi:10.3390/v13010044 (2020).
- 430 22 Hung, I. F. *et al.* Triple combination of interferon beta-1b, lopinavir-ritonavir, and
431 ribavirin in the treatment of patients admitted to hospital with COVID-19: an open-
432 label, randomised, phase 2 trial. *Lancet* **395**, 1695-1704, doi:10.1016/S0140-
433 6736(20)31042-4 (2020).
- 434 23 Lokugamage, K. G. *et al.* Type I Interferon Susceptibility Distinguishes SARS-CoV-2
435 from SARS-CoV. *J Virol* **94**, doi:10.1128/JVI.01410-20 (2020).
- 436 24 Pfaender, S. *et al.* LY6E impairs coronavirus fusion and confers immune control of viral
437 disease. *Nat Microbiol* **5**, 1330-1339, doi:10.1038/s41564-020-0769-y (2020).
- 438 25 Lei, X. *et al.* Activation and evasion of type I interferon responses by SARS-CoV-2.
439 *Nat Commun* **11**, 3810, doi:10.1038/s41467-020-17665-9 (2020).
- 440 26 Miorin, L. *et al.* SARS-CoV-2 Orf6 hijacks Nup98 to block STAT nuclear import and
441 antagonize interferon signaling. *Proc Natl Acad Sci U S A* **117**, 28344-28354,
442 doi:10.1073/pnas.2016650117 (2020).
- 443 27 Kopecky-Bromberg, S. A., Martinez-Sobrido, L., Frieman, M., Baric, R. A. & Palese,
444 P. Severe acute respiratory syndrome coronavirus open reading frame (ORF) 3b, ORF
445 6, and nucleocapsid proteins function as interferon antagonists. *J Virol* **81**, 548-557,
446 doi:10.1128/JVI.01782-06 (2007).
- 447 28 Nienhold, R. *et al.* Two distinct immunopathological profiles in autopsy lungs of
448 COVID-19. *Nat Commun* **11**, 5086, doi:10.1038/s41467-020-18854-2 (2020).
- 449 29 Sleijfer, S., Bannink, M., Van Gool, A. R., Kruit, W. H. & Stoter, G. Side effects of
450 interferon-alpha therapy. *Pharm World Sci* **27**, 423-431, doi:10.1007/s11096-005-1319-
451 7 (2005).
- 452

- 453 30 Stanifer, M. L. *et al.* Critical Role of Type III Interferon in Controlling SARS-CoV-2
454 Infection in Human Intestinal Epithelial Cells. *Cell Rep* **32**, 107863, doi:10.1016/j.celrep.2020.107863 (2020).
- 455 31 Vanderheiden, A. *et al.* Type I and Type III Interferons Restrict SARS-CoV-2 Infection
456 of Human Airway Epithelial Cultures. *J Virol* **94**, doi:10.1128/JVI.00985-20 (2020).
- 457 32 Scholer, L. *et al.* A Novel In-Cell ELISA Assay Allows Rapid and Automated
458 Quantification of SARS-CoV-2 to Analyze Neutralizing Antibodies and Antiviral
459 Compounds. *Front Immunol* **11**, 573526, doi:10.3389/fimmu.2020.573526 (2020).
- 460 33 Desmyter, J., Melnick, J. L. & Rawls, W. E. Defectiveness of interferon production and
461 of rubella virus interference in a line of African green monkey kidney cells (Vero). *J
462 Virol* **2**, 955-961, doi:10.1128/JVI.2.10.955-961.1968 (1968).
- 463 34 Jonsdottir, H. R. & Dijkman, R. Coronaviruses and the human airway: a universal
464 system for virus-host interaction studies. *Virology journal* **13**, 24, doi:10.1186/s12985-
465 016-0479-5 (2016).
- 466 35 Heinen, N., Klohn, M., Steinmann, E. & Pfaender, S. In Vitro Lung Models and Their
467 Application to Study SARS-CoV-2 Pathogenesis and Disease. *Viruses* **13**, doi:10.3390/v13050792 (2021).
- 468 36 V'Kovski, P. *et al.* Disparate temperature-dependent virus-host dynamics for SARS-
469 CoV-2 and SARS-CoV in the human respiratory epithelium. *PLoS Biol* **19**, e3001158, doi:10.1371/journal.pbio.3001158 (2021).
- 470 37 Megger, D. A., Philipp, J., Le-Trilling, V. T. K., Sitek, B. & Trilling, M. Deciphering
471 of the Human Interferon-Regulated Proteome by Mass Spectrometry-Based
472 Quantitative Analysis Reveals Extent and Dynamics of Protein Induction and
473 Repression. *Front Immunol* **8**, 1139, doi:10.3389/fimmu.2017.01139 (2017).
- 474 38 Trilling, M. *et al.* Deciphering the modulation of gene expression by type I and II
475 interferons combining 4sU-tagging, translational arrest and in silico promoter analysis.
476 *Nucleic Acids Res* **41**, 8107-8125, doi:10.1093/nar/gkt589 (2013).
- 477 39 Chen, P. *et al.* SARS-CoV-2 Neutralizing Antibody LY-CoV555 in Outpatients with
478 Covid-19. *N Engl J Med* **384**, 229-237, doi:10.1056/NEJMoa2029849 (2021).
- 479 40 Gottlieb, R. L. *et al.* Effect of Bamlanivimab as Monotherapy or in Combination With
480 Etesevimab on Viral Load in Patients With Mild to Moderate COVID-19: A
481 Randomized Clinical Trial. *Jama* **325**, 632-644, doi:10.1001/jama.2021.0202 (2021).
- 482 41 Consortium, W. H. O. S. T. *et al.* Repurposed Antiviral Drugs for Covid-19 - Interim
483 WHO Solidarity Trial Results. *N Engl J Med* **384**, 497-511, doi:10.1056/NEJMoa2023184 (2021).
- 484 42 Hadjadj, J. *et al.* Impaired type I interferon activity and inflammatory responses in
485 severe COVID-19 patients. *Science* **369**, 718-724, doi:10.1126/science.abc6027 (2020).
- 486 43 King, C. & Sprent, J. Dual Nature of Type I Interferons in SARS-CoV-2-Induced
487 Inflammation. *Trends Immunol* **42**, 312-322, doi:10.1016/j.it.2021.02.003 (2021).
- 488 44 Bastard, P. *et al.* Autoantibodies against type I IFNs in patients with life-threatening
489 COVID-19. *Science* **370**, doi:10.1126/science.abd4585 (2020).
- 490 45 Zhang, Q. *et al.* Inborn errors of type I IFN immunity in patients with life-threatening
491 COVID-19. *Science* **370**, doi:10.1126/science.abd4570 (2020).
- 492 46 Levy, R. *et al.* IFN-alpha2a Therapy in Two Patients with Inborn Errors of TLR3 and
493 IRF3 Infected with SARS-CoV-2. *J Clin Immunol* **41**, 26-27, doi:10.1007/s10875-020-
494 00933-0 (2021).
- 495 47 Troya, J. *et al.* Neutralizing Autoantibodies to Type I IFNs in >10% of Patients with
496 Severe COVID-19 Pneumonia Hospitalized in Madrid, Spain. *J Clin Immunol*,
497 doi:10.1007/s10875-021-01036-0 (2021).

- 502 48 Sa Ribero, M., Jouvenet, N., Dreux, M. & Nisole, S. Interplay between SARS-CoV-2
503 and the type I interferon response. *PLoS Pathog* **16**, e1008737,
504 doi:10.1371/journal.ppat.1008737 (2020).
- 505 49 Guo, K. *et al.* Qualitative Differences Between the IFNalpha subtypes and IFNbta
506 Influence Chronic Mucosal HIV-1 Pathogenesis. *PLoS Pathog* **16**, e1008986,
507 doi:10.1371/journal.ppat.1008986 (2020).
- 508 50 Schlaepfer, E. *et al.* Dose-Dependent Differences in HIV Inhibition by Different
509 Interferon Alpha Subtypes While Having Overall Similar Biologic Effects. *mSphere* **4**,
510 doi:10.1128/mSphere.00637-18 (2019).
- 511 51 Rusinova, I. *et al.* Interferome v2.0: an updated database of annotated interferon-
512 regulated genes. *Nucleic Acids Res* **41**, D1040-1046, doi:10.1093/nar/gks1215 (2013).
- 513 52 Meng, Z. *et al.* The effect of recombinant human interferon alpha nasal drops to prevent
514 COVID-19 pneumonia for medical staff in an epidemic area. *Curr Top Med Chem*,
515 doi:10.2174/1568026621666210429083050 (2021).
- 516 53 Hoagland, D. A. *et al.* Leveraging the antiviral type I interferon system as a first line of
517 defense against SARS-CoV-2 pathogenicity. *Immunity* **54**, 557-570 e555,
518 doi:10.1016/j.jimmuni.2021.01.017 (2021).
- 519 54 Hiemstra, P. S., McCray, P. B., Jr. & Bals, R. The innate immune function of airway
520 epithelial cells in inflammatory lung disease. *Eur Respir J* **45**, 1150-1162,
521 doi:10.1183/09031936.00141514 (2015).
- 522 55 Li, X., Wang, L., Nunes, D. P., Troxler, R. F. & Offner, G. D. Pro-inflammatory
523 cytokines up-regulate MUC1 gene expression in oral epithelial cells. *J Dent Res* **82**,
524 883-887, doi:10.1177/154405910308201107 (2003).
- 525 56 Chatterjee, M., van Putten, J. P. M. & Strijbis, K. Defensive Properties of Mucin
526 Glycoproteins during Respiratory Infections-Relevance for SARS-CoV-2. *mBio* **11**,
527 doi:10.1128/mBio.02374-20 (2020).
- 528 57 Sungnak, W. *et al.* SARS-CoV-2 entry factors are highly expressed in nasal epithelial
529 cells together with innate immune genes. *Nat Med* **26**, 681-687, doi:10.1038/s41591-
530 020-0868-6 (2020).
- 531 58 Zou, X. *et al.* Single-cell RNA-seq data analysis on the receptor ACE2 expression
532 reveals the potential risk of different human organs vulnerable to 2019-nCoV infection.
533 *Front Med* **14**, 185-192, doi:10.1007/s11684-020-0754-0 (2020).
- 534 59 Lu, W. *et al.* Elevated MUC1 and MUC5AC mucin protein levels in airway mucus of
535 critical ill COVID-19 patients. *J Med Virol* **93**, 582-584, doi:10.1002/jmv.26406 (2021).
- 536 60 Jonsdottir, H. R. & Dijkman, R. Characterization of human coronaviruses on well-
537 differentiated human airway epithelial cell cultures. *Methods Mol Biol* **1282**, 73-87,
538 doi:10.1007/978-1-4939-2438-7_8 (2015).
- 539 61 Livak, K. J. & Schmittgen, T. D. Analysis of relative gene expression data using real-
540 time quantitative PCR and the 2(-Delta Delta C(T)) Method. *Methods* **25**, 402-408,
541 doi:10.1006/meth.2001.1262 (2001).
- 542 62 Hu, J., Ge, H., Newman, M. & Liu, K. OSA: a fast and accurate alignment tool for
543 RNA-Seq. *Bioinformatics* **28**, 1933-1934, doi:10.1093/bioinformatics/bts294 (2012).
- 544 63 Love, M. I., Huber, W. & Anders, S. Moderated estimation of fold change and
545 dispersion for RNA-seq data with DESeq2. *Genome Biol* **15**, 550, doi:10.1186/s13059-
546 014-0550-8 (2014).
- 547 64 Kramer, A., Green, J., Pollard, J., Jr. & Tugendreich, S. Causal analysis approaches in
548 Ingenuity Pathway Analysis. *Bioinformatics* **30**, 523-530,
549 doi:10.1093/bioinformatics/btt703 (2014).
- 550 65 Ianevski, A., He, L., Aittokallio, T. & Tang, J. SynergyFinder: a web application for
551 analyzing drug combination dose-response matrix data. *Bioinformatics* **33**, 2413-2415,
552 doi:10.1093/bioinformatics/btx162 (2017).

553 **Methods**

554 **Stimulation with different human IFN α subtypes**

555 IFN α subtypes were produced and purified as previously described ⁷. The activity of each
556 subtype was determined using the human ISRE-Luc reporter cell line, a retinal pigment
557 epithelial cell line transfected with a plasmid containing the Firefly Luciferase gene, stably
558 integrated under control of the IFN-stimulation-response element (ISRE). Following
559 stimulation with IFN α , chemiluminescence can be detected and used to calculate the respective
560 activity in units against commercially available IFN α (PBL assays sciences, Piscataway,
561 USA)⁷.

562

563 **End-point dilution assay**

564 VeroE6 cells were seeded at a density of 10,000 cells per well in a 96-well plate and maintained
565 in 200 μ l DMEM (Gibco) supplemented with 10% fetal bovine serum (Sigma-Aldrich), L-
566 glutamine (Gibco), penicillin and streptomycin (Gibco) overnight. The next day, 22 μ l of virus
567 stock or apical washes of hAEC were added to the first row of the plate (6 replicates). Then,
568 the virus was diluted 1:10 by mixing the media and pipetting 22 μ l to the next row repeatedly,
569 followed by 72 h incubation in 37°C in a 5% CO₂ atmosphere. Thereafter, the supernatant was
570 aspirated and the cells were incubated in 100 μ l of crystal violet solution (0.1 % crystal violet
571 (Roth) in PBS, 10% ethanol, 0.37% formalin) for 5 min. Subsequently, the crystal violet
572 solution was aspirated, cells were washed with PBS and the number of wells with intact or
573 damaged cell layer were determined. The TCID₅₀/mL was calculated by the Spearman & Kärber
574 algorithm.

575

576 **IFN titration assay**

577 VeroE6 cells were seeded at a density of 10,000 cells per well in a 96-well plate and maintained
578 in DMEM supplemented with 10% fetal bovine serum, L-glutamine, penicillin and

579 streptomycin overnight. Then, the medium was aspirated and serially diluted IFN α and IFN λ 3
580 (R&D Systems) and virus with a final concentration of 350 PFU/mL were added to the cells in
581 a total volume of 100 μ l of cell culture media, followed by 72 h incubation in 37°C in a 5%
582 CO₂ atmosphere. Thereafter, the supernatant was aspirated and the cells were incubated in 100
583 μ l of crystal violet solution (0.1 % crystal violet in PBS, 10% ethanol, 0.37% formalin) for 5
584 min. Subsequently, the crystal violet solution was aspirated, cells were washed with PBS and
585 the number of wells with intact or damaged cell layer were determined.

586 The inhibitory concentration 50 (IC50) was calculated using GraphPad Prism 6.

587

588 **In-cell ELISA**

589 The in-cell (ic) ELISA was performed based on the previously published protocol (Scholer et
590 al., 2020). VeroE6 cells were seeded at a density of 20,000 cells per well in a 96-well plate and
591 maintained in DMEM supplemented with 10% fetal bovine serum, L-glutamine, penicillin and
592 streptomycin. At indicated time points, the medium was aspirated and serially diluted IFN α or
593 the indicated concentrations of remdesivir and virus with a final concentration of 350 PFU/mL
594 were added to the cells in a total volume of 100 μ l, followed by 24 h incubation in 37°C in a
595 5% CO₂ atmosphere. Thereafter, 100 μ l of 8% ROTI®Histofix (Roth) (equals 4% of total PFA)
596 were added for a minimum of 2 h at room temperature to fix the cells and inactivate the virus.
597 Afterwards, the plate was washed thrice with PBS. The PBS was aspirated and 200 μ l of freshly
598 prepared permeabilization buffer (PBS, 1% Triton X-100 (Roth)) were added to the cells and
599 the plate was incubated for 30 min at room temperature with constant shaking. Subsequently,
600 the permeabilization buffer was aspirated and 200 μ l of blocking buffer (PBS, 3% FBS) were
601 added for 1 h. Then, the blocking buffer was aspirated and 50 μ l of primary antibody solution
602 (anti-SARS-CoV-2-NP (RRID: AB_2890255) 1:5000 diluted in PBS + 1% FBS) was added to
603 each well. The plate was incubated overnight at 4°C. The next day, the primary antibody
604 solution was aspirated and the plate was washed thrice with wash buffer (PBS, 0.05% Tween

605 20 (Roth)). Thereafter, 50 μ l of the secondary antibody solution (Peroxidase-AffiniPure Goat
606 Anti-Mouse IgG (H+L) (RRID: AB_10015289) 1:2000 in PBS, 1% FBS) was added to the
607 wells and the plate was incubated for 2 h at room temperature. After the incubation period, the
608 wells were washed 4 times with 250 μ l wash buffer. Afterwards 100 μ l of TMB substrate
609 solution (BioLegend) were added and the plate was incubated about 20 min at room temperature
610 in the dark. The reaction was stopped by addition of 100 μ l 2N H₂SO₄ (Roth). The absorbance
611 was measured at 450 nm with a reference wavelength of 620 nm using Spark® 10M multimode
612 microplate reader (Tecan).

613

614 **Cell viability assay**

615 To exclude cytotoxic effects of the compounds used in our assays, a cell viability assay was
616 performed using the Orangu™ Cell Counting Solution (CELL guidance systems) according to
617 the manufacturer's instructions. The cells were seeded and treated equally to the protocol that
618 was used before without any viral infection. Afterwards, 10 μ l of Orangu™ Cell Counting
619 Solution were added to each well and the plate was incubated for 2 h. Then, the absorbance was
620 measured at 450 nm with Spark® 10M multimode microplate reader.

621

622 **Immunofluorescence**

623 VeroE6 cells were seeded and treated as described for the in-cell ELISA. After incubation with
624 the primary antibody solution, 50 μ l secondary antibody solution (Goat IgG anti-Mouse IgG
625 (H+L)-Alexa Fluor 488, MinX none 1:2000 (RRID: AB_2338840), Phalloidin CF647 1:100
626 (Biotium) in PBS + 1% FBS) were added to each well and the plate was incubated for 2 h at
627 room temperature. Thereafter, the secondary antibody solution was aspirated and the cells were
628 counterstained for 20 min at room temperature with 50 μ l of DAPI solution (0.1 μ g/mL DAPI
629 (Sigma-Aldrich) in PBS). Subsequently, the plate was washed thrice with PBS and
630 microscopically analyzed using Leica THUNDER Imager 3D Cell Culture.

631

632 **Infection of Human airway epithelial cells**

633 Human airway epithelial cells (hAEC) were obtained from lung transplant donors post mortem
634 (ethics of University Duisburg- Essen (18-8024-BO and 19-8717-BO)) or from explanted lungs
635 (Ethics of Hannover medical school 3346/2016. Selection criteria for donors are listed in the
636 Eurotransplant guidelines. hAECs from explanted lungs were cultured and differentiated as
637 previously described ⁶⁰ hAEC from lung transplant donors post mortem were obtained by the
638 following protocol: During the adaptation of the donor lung, a small tracheal ring was removed
639 and stored in PBS supplemented with antibiotics (penicillin 100 U/mL, streptomycin 100
640 µg/mL, 10 µg/mL ciprofloxacin (Kabi)). HAEc were isolated from the mucosa within 24 h
641 after transplantation by enzymatic digestion (Protease XIV (Sigma Aldrich)) and scraping.
642 Cells were expanded for 7-14 days in KSFm (keratinocyte-SF-medium (Gibco), supplemented
643 with human epidermal growth factor (Gibco) (2.5 ng/mL), bovine pituitary extract (Gibco)
644 (BPE 25 µg/mL, Gibco), isoproterenol (Sigma-Aldrich) (1µM), Penicillin, Streptomycin,
645 Ciprofloxacin, Amphotericin B (PanBiotech) (2,5 µg/mL)) and after trypsinization stored in
646 liquid nitrogen (10% DMSO, 90% KSFm+BPE 0,3mg/mL). All plastic surfaces during hAEC
647 isolation and air liquid interface (ALI) culture were coated with human fibronectin (PromoCell)
648 (5 µg/mL), type I bovine collagen (Advanced BioMatrix) (PureCol 30 µg/mL) and BSA (10
649 µg/mL). For ALI cultures, cells were thawed, expanded in KSFm for 5-7 days and transferred
650 to transwell inserts (PE Membrane, 12 well plates, 0.4 µm pore size, Corning). A monolayer
651 hAECs were grown submerged in S/D Media (1:1 mixture of DMEM (StemCell) and BEpiCM-
652 b (ScienCell), supplemented with Penicillin and Streptomycin, HEPES (Gibco) (12.5mL/l,
653 1M), 1x Bronchial Epithelial Cell Growth Supplement (ScienCell), and EC-23 (Tocris) (5mM)
654 until they reached confluence. Apical media was removed and cell differentiation was induced
655 under air exposure for 2 weeks. Infection was started after cells were fully differentiated

656 measured by movement of cilia, secretion of mucus and transepithelial electrical resistance
657 ($>1000\Omega/\text{cm}^2$).

658 Fully differentiated hAECs were washed with HBSS apically for 10 min before infection. For
659 SARS experiments, the cells were infected apically with 30,000 PFU diluted in HBSS, for
660 Influenza, the cells were apically infected with Influenza A virus H1H1 strain A/Puerto Rico/34
661 (PR8) at 0.1 MOI in 200 μl HBSS. The cells were incubated with the inoculum for 1 h in 33°C
662 in a 5 % CO₂ atmosphere. Thereafter, the inoculum was aspirated and the cells were washed
663 thrice with 150 μl of HBSS for 10 min. The last wash was collected and stored at -80 °C as 0 h
664 sample. At the indicated time points, cells were washed apically for 10 min and the washes
665 were subjected to an end-point dilution assay or to a plaque titration assay as described for
666 SARS-CoV-2 and Influenza, respectively.

667 Treatment of hAECs was performed by adding the indicated amounts of IFNs or remdesivir
668 directly to the cell culture medium on the basolateral side of the cells.

669 For the isolation of RNA, cells were lysed using Qiagen RLT buffer (Qiagen) supplemented
670 with 1% β -mercaptoethanol (Sigma-Aldrich).

671

672 **Viral mRNA quantification**

673 Total RNA was purified from hAECs and VeroE6 cells using the RNeasy Mini Kit (Qiagen)
674 according to manufacturer's instructions with preceding DNase I digestion with the RNase-
675 Free DNase Set (Qiagen).

676 To determine relative SARS-CoV-2 M- or N-gene expression, 500 ng of total RNA were
677 reverse transcribed using the PrimeScript™ RT Master Mix (Takara). Promega's GoTaq®
678 Probe qPCR Master Mix was used according to the manufacturer's instructions with gene
679 specific primers and probes (see Extended data table 7). RT-qPCR was performed on a
680 LightCycler® 480 II (Roche) instrument, with the following conditions: initial denaturation
681 was 2 min at 95 °C and a ramp rate of 4.4 °C/s, followed by 40 cycles of denaturation for 15

682 seconds at 95 °C and a ramp rate of 4.4 °C/s and amplification for 60 seconds at 60°C and a
683 ramp rate of 2.2 °C/s. To assess M- and N-gene copy numbers, the M- and N-gene were partially
684 cloned into pCR™2.1 (ThermoFisher Scientific) or pMiniT 2.0 (NEB), respectively, and a 1:10
685 plasmid dilution series was used as a reference.

686

687 **IAV plaque assay**

688 MDCK-II cells were seeded in 6 well plates, and cultured in DMEM supplemented with 5%
689 FBS and 1% Penicillin-Streptomycin until 100% confluent. On the day of infection, 10-fold
690 dilutions of apical washes were prepared in infection-PBS (PBS supplemented with 1%
691 Penicillin-Streptomycin, 0.01% CaCl₂, 0.01% MgCl₂ and 0.2% BSA). Cells were washed once
692 with infection-PBS, infected with 500 µl of diluted samples (virus inoculum), and were
693 incubated at 37°C, 5% CO₂ for 30 min. The inoculum was removed, and the infected monolayer
694 was overlaid with plaque medium (prepared immediately before use by mixing 14.2% 10X
695 MEM (Gibco), 0.3% NaHCO₃, 0.014% DEAE-Dextran (Sigma-Aldrich), 1.4% 100X
696 Penicillin-Streptomycin, 0.3% BSA, 0.9% Agar, 0.01% MgCl₂, 0.01% CaCl₂, 0.15 mg TPCK-
697 Trypsin (Sigma). Plates were kept at room temperature until the agar solidified, and were
698 incubated upside down at 37°C, 5% CO₂ for 72h. Plaques were quantified in terms of infectious
699 IAV particles, and were represented as PFU/mL.

700

701 **ISG expression**

702 500,000 VeroE6 cells were seeded and stimulated with 1000 U/mL of IFN α subtypes 5, 7, 16,
703 or 1000 ng/mL IFN λ 3 for 16 h. Afterwards, the cells were lysed using DNA/RNA Shield for
704 RNA isolation.

705 RNA was isolated from cell lysates with Quick-RNA™ Miniprep Kit (Zymo Research)
706 according to the manufacturer's instruction.

707 CDNA was synthesized from isolated RNA using cDNA Synthesis Super Mix (Bimake)
708 according to the manufacturer's instructions. ISG expression levels were quantified by qPCR
709 with Luna® Universal qPCR Master Mix and the respective primer pairs (see Extended data
710 table 6). Expression levels were normalized by 2- $\Delta\Delta CT$ method⁶¹ using GAPDH as reference
711 gene.

712

713 **Proteomics sample preparation**

714 Cells were washed with ice cold PBS and harvested in urea buffer (30 mM Tris HCl, 7 M Urea,
715 2 M Thiourea, 0.1% NaDOC, pH 8.5). Cells were centrifuged for 15 min at 16,100 x g and 4
716 °C and the supernatant was further processed.

717 Tryptic digestion was performed on 20 µl cell lysate. Disulfide bonds were reduced by adding
718 final 5 mM DTT (Dithiothreitol) for 15 minutes at 50 °C before thiols were alkylated by final
719 15 mM IAA (iodoacetamide) for 15 min in the dark. Hydrophilic and hydrophobic Cytiva Sera-
720 Mag Carboxyl-Magnet-Beads (GE Healthcare) were mixed 1:1 and 2 µl beads (25 µg/µl) were
721 added per samples. The samples were filled up to 70% ACN (acetonitrile) and incubated for 15
722 min to ensure protein binding to the beads. Subsequently, beads were washed two times with
723 70% EtOH followed by washing with 100% ACN. Beads were resuspended in 100 mM
724 ammonium bicarbonate containing 0.2 µg trypsin (SERVA) per sample and
725 incubated overnight at 37 °C. The peptides were transferred into a new reaction tube, vacuum
726 dried and dissolved in 0.1 % TFA (trifluoroacetic acid).

727

728 **LC-MS/MS Analysis**

729 400 ng tryptic peptides per sample were analyzed using an Ultimate 3000 RSLCnano HPLC
730 (Dionex) coupled to a Q Exactive HF Orbitrap (Thermo Fisher Scientific). Samples were pre-
731 concentrated on a C18 trap column (Acclaim PepMap 100; 100 µm × 2 cm, 5 µm, 100 Å;
732 Thermo Fisher Scientific) within seven minutes at a flow rate of 30 µL/min with 0.1 % trifluoric

733 acid and subsequently transferred to a Nano Viper C18 analytical column (Acclaim PepMap
734 RSLC; 75 μ m \times 50 cm, 2 μ m, 100 \AA ; Thermo Fisher Scientific). Peptide separation was
735 performed by a gradient from 5% - 30% solvent B over 120 minutes at 400 nL/min (solvent A:
736 0.1% formic acid; solvent B: 0.1% formic acid, 84% acetonitrile). Full-scan mass spectra were
737 acquired in profile mode at a resolution of 70,000 at 400 m/z within a mass range of 350 – 1400
738 m/z. The 10 highest abundant peptide ions were fragmented by HCD (NCE [normalized
739 collision energy] = 27) and MS/MS spectra were acquired at a resolution of 35,000.

740

741 **Proteomics Data Analysis**

742 Peptide identification and quantification were performed using MaxQuant (v.1.6.17) searching
743 UniProtKB/SwissProt (2020_05, 563,552 entries) restricted to either *Homo sapiens* or *Homo*
744 *sapiens* and SARS-CoV-2. Search parameters were default, LFQ was used for peak
745 quantification and normalization was enabled. Peptides were considered for quantification
746 irrespective of modifications. Match between runs was enabled when the analysis was
747 performed considering human proteins only. Statistical data analysis was conducted using R
748 (v.3.6.2). Differences between the experimental groups were assessed using t-tests (paired, two-
749 sided) and proteins quantified in minimum 3 of 4 donors per group with minimum 2 unique
750 peptides, a p-value ≤ 0.05 and a ratio of mean abundances ≥ 1.5 or ≤ 0.67 were considered
751 statistically significant. Proteins that were quantified in one experimental group but not detected
752 at all in an opposed group were defined as On-Offs between these groups. GO annotation and
753 enrichment analyses were performed using STRING (v.11). Data visualization was done using
754 R and Cytoscape (v.3.8.2).

755

756 **Data availability**

757 The authors declare that the data supporting the findings of this study are available within the
758 article and its Extended Data files or are available on request. The mass spectrometry

759 proteomics data have been deposited at the ProteomeXchange consortium via the PRIDE
760 partner repository with the dataset identifier PXD000XXX.

761

762 **Transcriptomics**

763 Quality and integrity of total RNA was controlled on 5200 Fragment Analyzer System (Agilent
764 Technologies)). The RNA sequencing library was generated from 50 ng total RNA using
765 NEBNext® Single Cell/Low Input RNA Library to manufacture´s protocols. The libraries were
766 treated with Illumina Free Adapter Blocking and were sequenced on Illumina NovaSeq 6000
767 using NovaSeq 6000 S1 Reagent Kit (100 cycles, paired end run 2x 50 bp) with an average of
768 3×10^7 reads per RNA sample.

769

770 **Transcriptomic analysis**

771 FASTQ files of RNA sequencing files were imported into the Array Studio software v10.2.5.9
772 (QIAGEN, Cary, NC, USA) package for further data analysis. All FASTQ files were aligned
773 to the gene model Ensembl v96 and to the reference library Human B38 using the proprietary
774 OmicSoft Aligner OSA⁶². Differential gene expression of each condition was assessed using
775 DESeq2⁶³. Differentially expressed genes were sent to Ingenuity Pathway Analysis (IPA)
776 ([https://digitalinsights.qiagen.com/products-overview/discovery-insights-portfolio/analysis-](https://digitalinsights.qiagen.com/products-overview/discovery-insights-portfolio/analysis-and-visualization/qiagen-ipa/)
777 [and-visualization/qiagen-ipa/](https://digitalinsights.qiagen.com/products-overview/discovery-insights-portfolio/analysis-and-visualization/qiagen-ipa/)) for biological analysis using the cutoffs: p-value <0.05, fold
778 change (fc) $>|1.5|$ and mean counts min>5. IPA statistics is based on two outputs. A p-value
779 derived from a right-tailed Fisher's Exact Test estimates the probability that the association
780 between a function or pathway and a set of molecules might be due to random chance but does
781 not consider directional changes. This is, however, predicted for a disease and/or function,
782 canonical pathway, or upstream regulator (activation or inhibition) by the activation z-score
783 algorithm. The z-score describes the number of standard deviations data lies above or below
784 the mean. A z-score >2 was considered significantly increased whereas a z-score<-2 was

785 considered significantly decreased⁶⁴. We performed an expression analysis to evaluate
786 transcriptomic changes for Canonical Pathways in each of the comparison IFN vs mock⁶⁴.

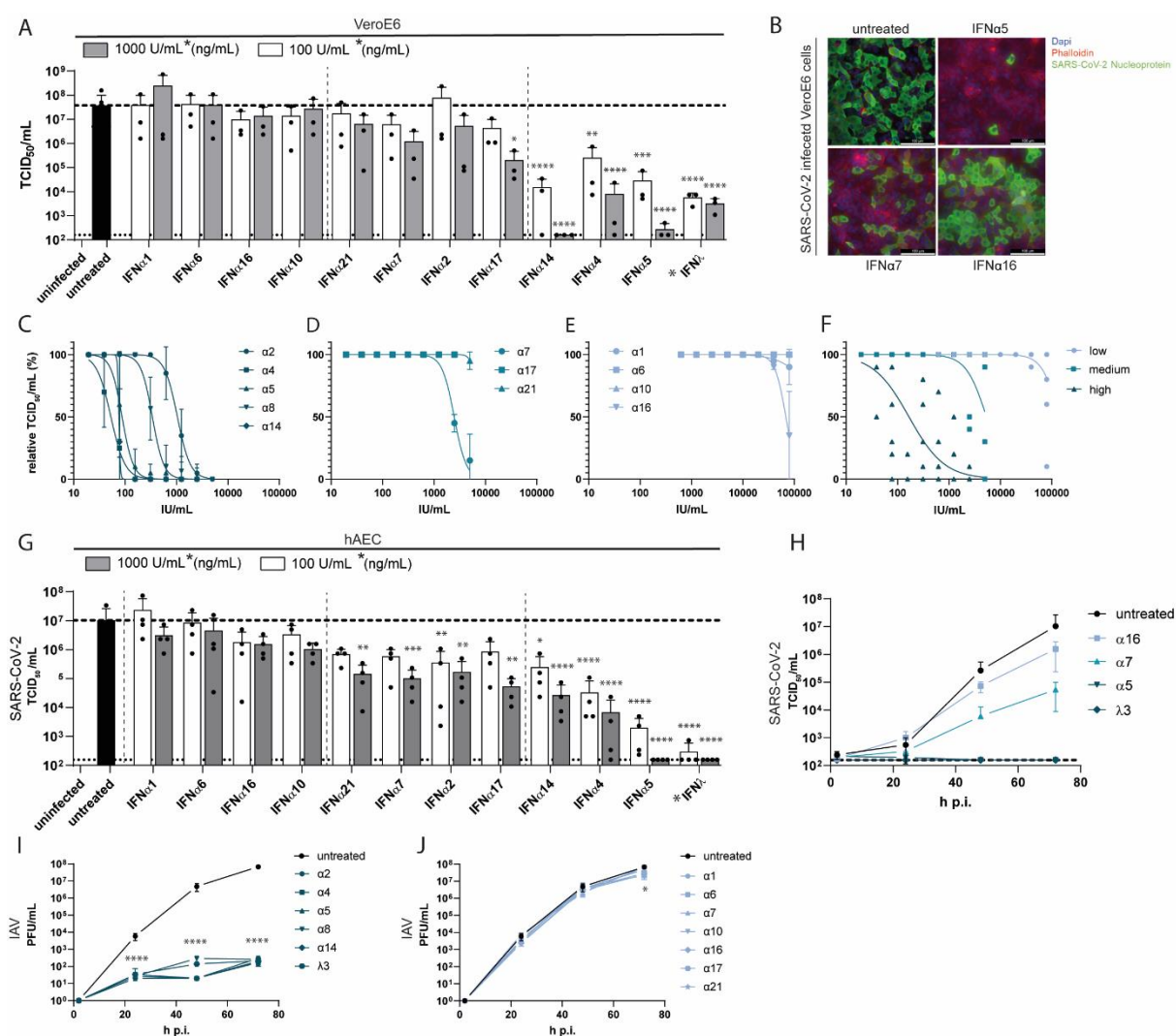
787

788 **Statistical analysis**

789 Differences in transformed data were tested for significance using GraphPad Prism v8.4.2 for
790 Windows (GraphPad). Statistically significant differences between the IFN α -treated groups and
791 the untreated group were analyzed using Ordinary One-Way ANOVA analysis with Dunnett's
792 multiple comparison test. P values < 0.05 were considered significant.

793

794 **Figures and Figure Legends**

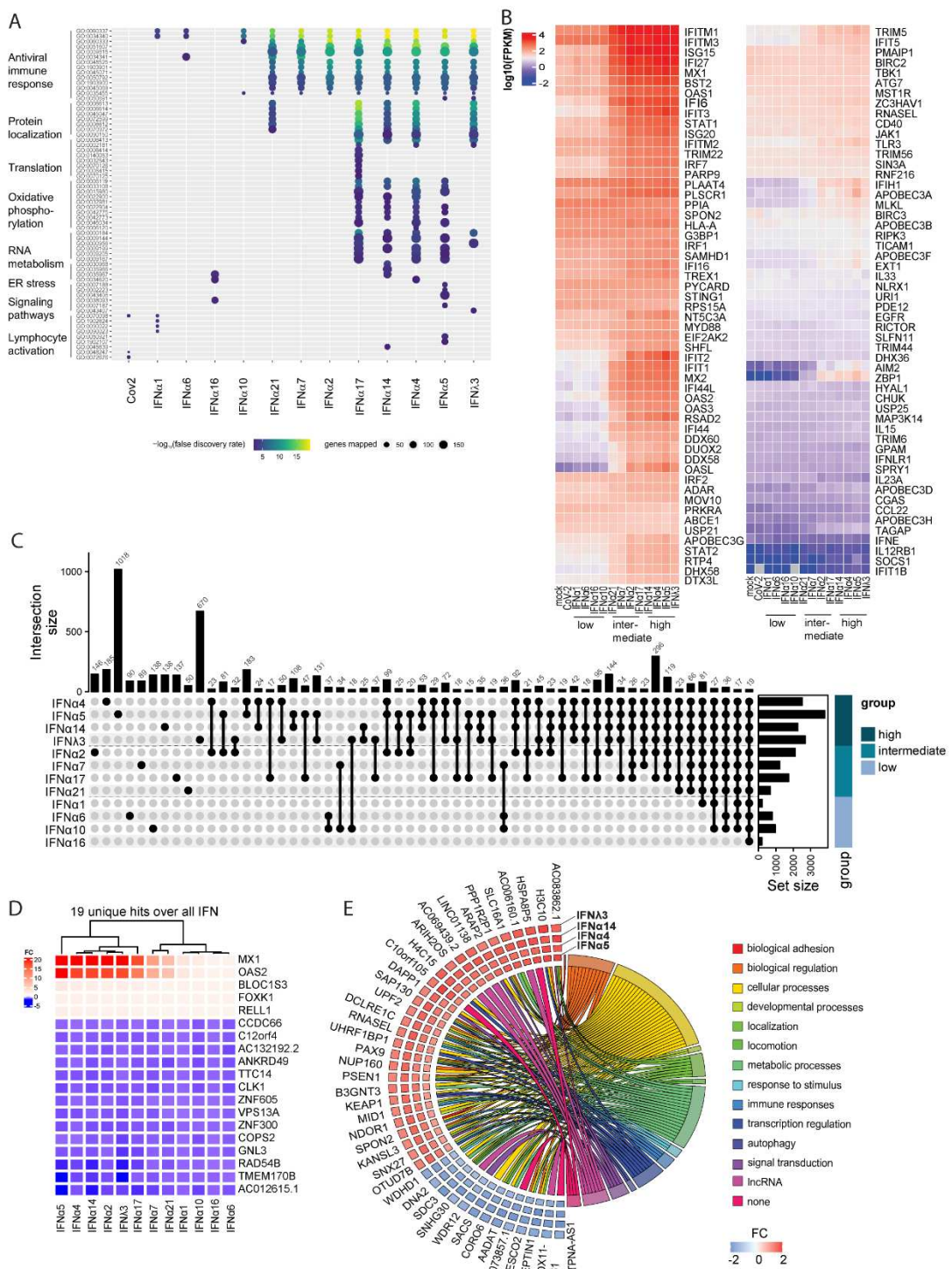


795
796 **Fig. 1: Treatment with IFN α subtypes reveals distinct antiviral effects against SARS-CoV-
797 2**

798 (A) Antiviral activity of IFN α subtypes (100 or 1000 U/mL) and IFN λ 3 (100 or 1000 ng/mL)
799 against SARS-CoV-2 on VeroE6 cells (TCID₅₀/mL). (B) Representative immunofluorescence
800 staining of IFN-treated SARS-CoV-2 infected VeroE6 cells. IFN α subtypes were titrated
801 against SARS-CoV-2 on VeroE6 cells by TCID₅₀ assay and the IFNs were grouped in high (C),
802 medium (D) and low (E) antiviral pattern and the mean values of each group are plotted in (F).
803 Antiviral activity of IFN α subtypes and IFN λ 3 in SARS-CoV-2-infected primary hAECs at 72
804 h p.i. (G) and kinetics of four selected IFNs (H). (I-N) Antiviral activity of IFN α subtypes and
805 IFN λ 3 in Influenza A/PR8-infected primary hAECs at different timepoints post infection. Mean

806 values of high (I) and low/not (J) antiviral IFNs are shown. (A, C-F; I, J) Mean values \pm SEM
807 are shown for n=3. (G, H) n=4. A: 100 U/mL (ng/mL): ** p=0.0035 (IFN α 4); *** p=0.0002
808 (IFN α 5); **** p<0.0001 (IFN α 14, IFN λ 3); 1000 U/mL (ng/mL): * p=0.0180 (IFN α 17); ****
809 p<0.0001 (IFN α 4, α 5, α 14, λ 3). G: 100 U/mL (ng/mL): * p=0.0352 (IFN α 14); ** p=0.0063
810 (IFN α 2) *** p=0.0002 (IFN α 4); **** p<0.0001 (IFN α 5, IFN λ 3); 1000 U/mL (ng/mL): **
811 p=0.0028 (IFN α 2) p=0.0016 (IFN α 17) p=0.0021 (IFN α 21) *** p=0.0003 (IFN α 7); ****
812 p<0.0001 (IFN α 4, α 5, α 14, λ 3); I: **** p<0.0001 (all IFNs, all time points J. 72hpi * p=0.0468
813 (IFN α 16)

814



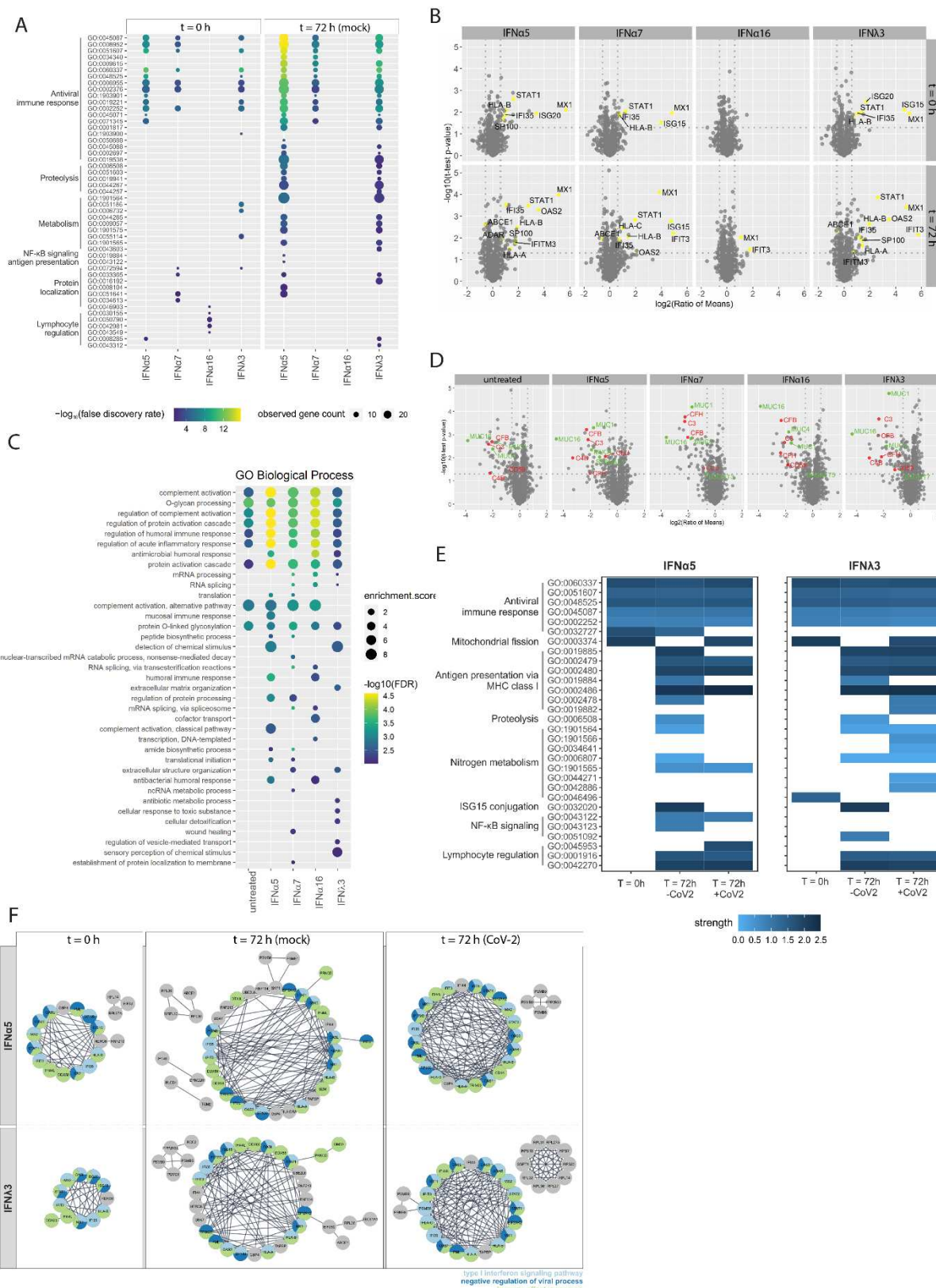
815

816 Fig.2: Transcriptomic analysis display IFN subtype specific immune signatures

817 (A-E) Transcriptomic analyses of IFN-treated (16 hours post treatment; 1000U/mL or
818 1000ng/mL) or SARS-CoV-2-infected (18 hours post infection) hAECs. (A) Biological
819 processes induced by IFNs or SARS-CoV-2. (B) Heat maps displaying genes contained in
820 antiviral response. (C) UpSet plots to summarize key differentially expressed genes (DEG).
821 Numbers of individually or group-specific DEGs are shown as bars and numbers. The bottom

822 right horizontal bar graph labelled Set Size shows the total number of DEGs per treatment.
823 IFNs are plotted due to their antiviral activity in 3 groups (high, medium and low). (D)
824 Heatmap of the 19 basal DEGs expressed by all IFNs as identified in D. (E) Plot depicting
825 fold changes (FC) of identified 42 unique genes in the group displaying high antiviral activity
826 and association of genes to functional categories.
827 (A-E) n=4

828



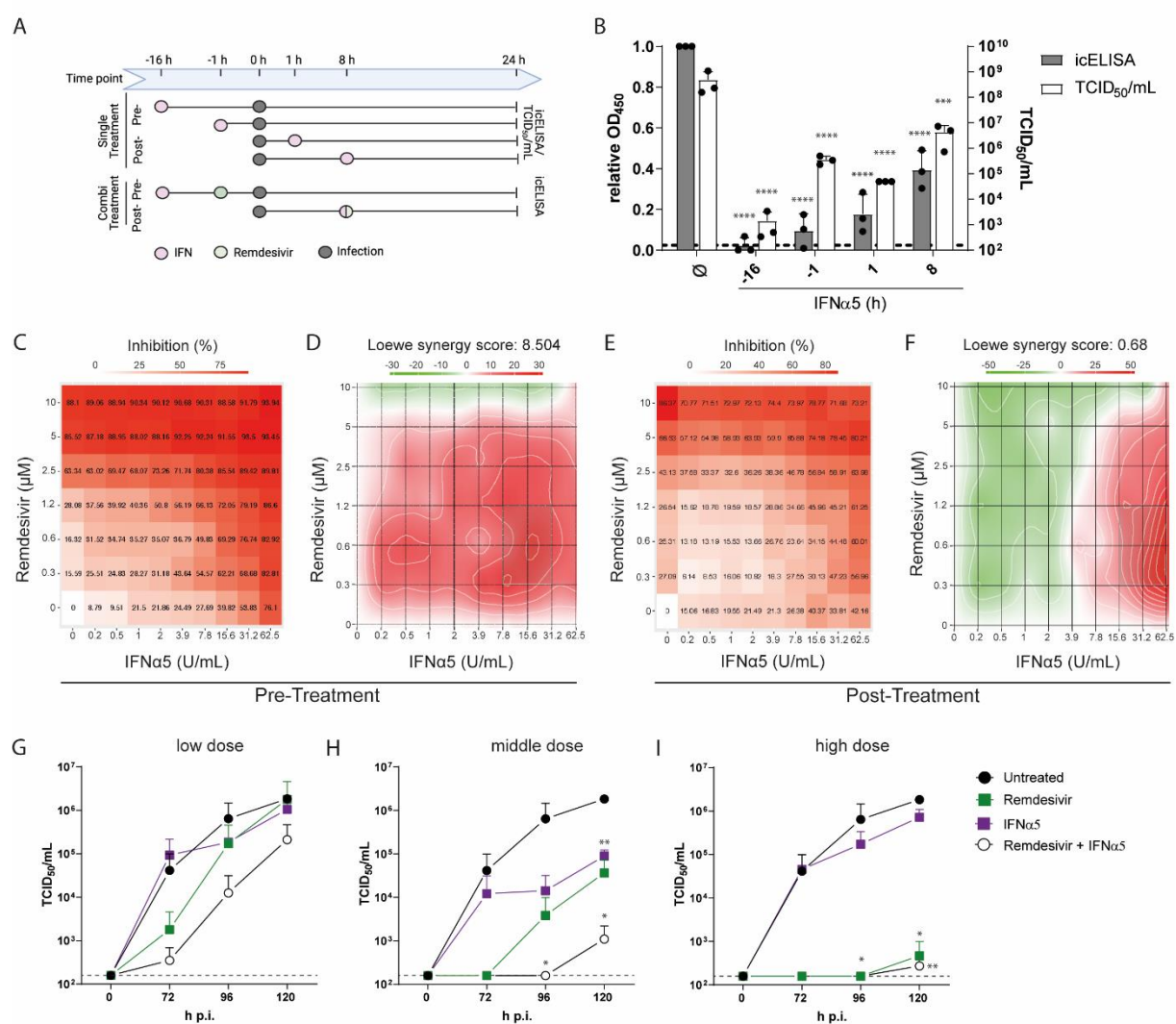
829

830 **Fig. 3: Proteomic analysis highlights key cellular mediators**

831 (A-G) Proteomic analysis of IFN-treated (1000U/mL or 1000ng/mL) and/or SARS-CoV-2-
832 infected hAECs. (A) Biological processes induced by IFNs 16 hours post treatment (t=0 h) or

833 88 hours post treatment (t=72 h). (B) Volcano plots of IFN-treated hAECs at different
834 timepoints post treatment. Detected ISGs are coloured yellow. (C) Biological processes induced
835 by IFNs 88 hours post treatment in the presence of SARS-CoV-2 (t=72 h) (D) Volcano plots of
836 IFN-treated SARS-CoV-2-infected hAEC. Detected proteins are coloured due to their
837 biological function: red = complement activation; green =O-glycan processing. (E) Heatmaps
838 of differentially activated biological processes by highly antiviral IFN α 5 and IFN λ 3 compared
839 to untreated controls at different time-points post treatment in the presence and absence of
840 SARS-CoV-2. (F) STRING analysis of proteins increased in IFN-treated and/or SARS-CoV-2
841 infected hAECs and identified abundant protein-protein interactions. Proteins shown as circles
842 and colours indicating biological processes (A-F) n=4.

843



844

845 **Fig. 4: Therapeutic potential of highly antiviral IFN α subtype 5**

846 (A-F) Single and combined treatments of IFN α 5 and remdesivir in SARS-CoV-2 infected
 847 VeroE6 cells. (A) Schematic depiction of treatment. (B) Pre- and post-treatments of VeroE6
 848 cells by icELISA (grey bars) and TCID₅₀ assay (white bars). (C) Inhibition of SARS-CoV-2
 849 infection and (D) analysis of drug combination experiments using SynergyFinder web
 850 application 16 hours before infection. (E) Inhibition of SARS-CoV-2 infection and (F) analysis
 851 of drug combination experiments using SynergyFinder web application⁶⁵ (doi: 10.1093/bioinformatics/btx162) 8 hours post infection. (G-I) remdesivir and IFN α 5
 852 combinational treatment 8 hours post infection of hAECs with low doses (0.313 μ M remdesivir,
 853 0.2444 U/mL IFN α 5; G), medium doses (0.63 μ M remdesivir, 15.625 U/mL IFN α 5; H) and

855 high doses (2.5 μ M remdesivir, 1.953 U/mL IFN α 5; I) (B-I) n=3. B: icELISA (grey bars) ****

856 p<0.0001; TCID50/mL (white bars) *** p=0.0003 (+8) **** p<0.0001 (-16, -1, +1) H: 96h p.

857 i. * p=0.0205 (remdesivir + IFN α 5);120h p. i. * p=0.0113 (remdesivir + IFN α 5) ** p=0.0041

858 (IFN α 5) I: 96h p. i. * p=0.0205 (remdesivir, remdesivir + IFN α 5);120h p. i. ** p=0.0081

859 (remdesivir) ** p=0.0015 (remdesivir + IFN α 5)

860

861 Acknowledgements

862 We would like to thank all member of the Department for Molecular and Medical Virology of
863 the Ruhr University Bochum for helpful suggestions and discussion. We thank Kristin Fuchs
864 and Birgit Zülch for excellent technical assistance. We want to thank the Westdeutsche Biobank
865 Essen (WBE, University Hospital Essen, University of Duisburg-Essen, Essen, Germany;
866 approval WBE-ref. 20-WBE-102) for providing Human biological samples.

867 Author Contributions

868 S.P., K.S., E.S., U.D., D.T., designed the project. J. S., T.L.M., K.S., C.E., N.H., Z.K., S.H.,
869 S.K., L.B., B.W., H.B., A.K. performed and analysed experiments. D.T. T.B., K.Sch., J.N.B.,
870 and M.E. performed statistical analysis and data analysis. T.P., B.S., J.C., Z.Y., C.T.,
871 V.T.K.L.T., M.T. and S.L. contributed to the design and implementation of the research. S.P.,
872 and K.S., wrote the manuscript, and all authors contributed to editing.

873

874 Competing interest declaration

875 The authors declare no competing interests. J.N.B. is an employee of QIAGEN, Inc. (no conflict
876 of interest).

877

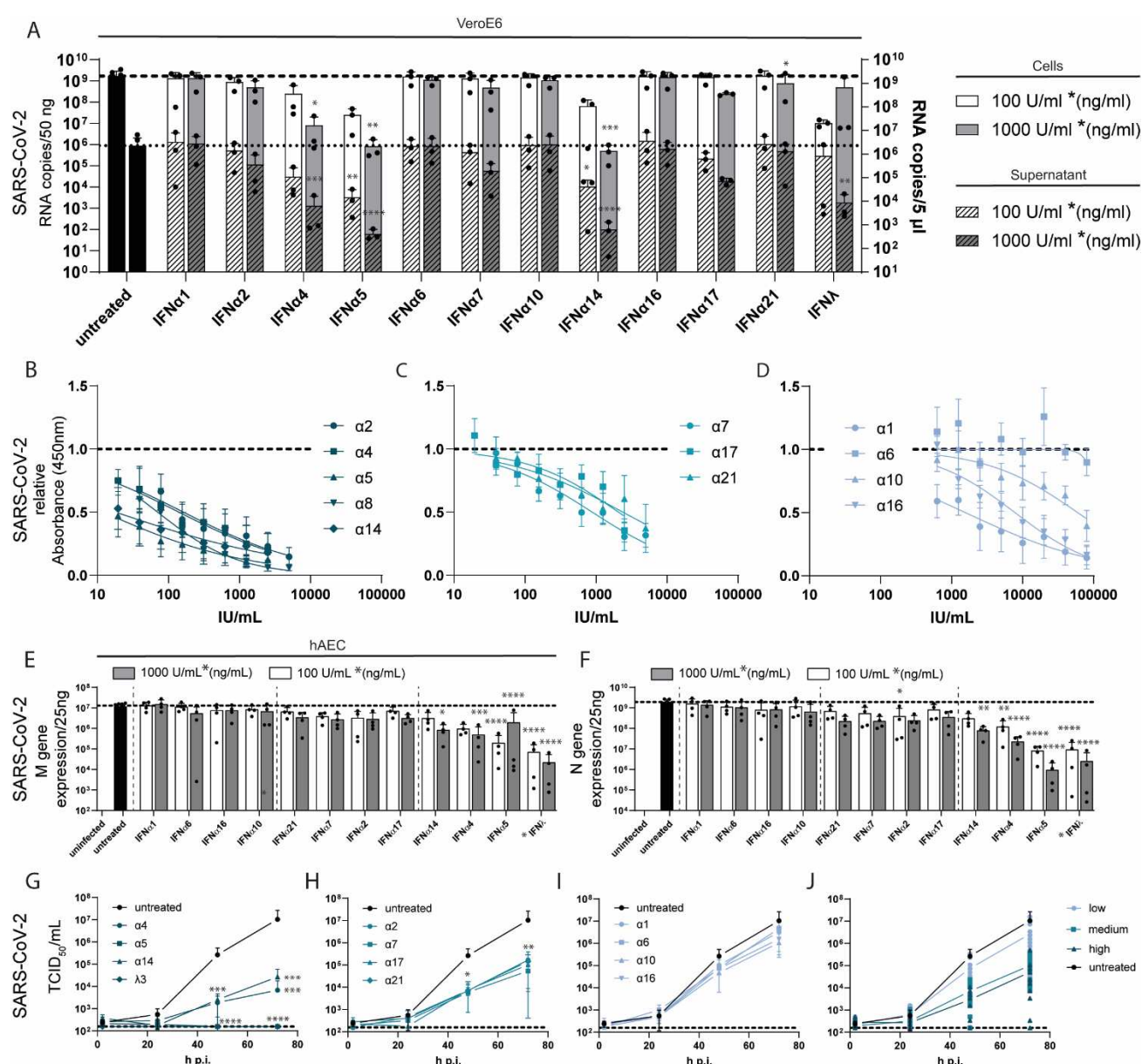
878 Funding

879 K.S. was supported by a grant from the DFG (SU1030-2-1) and Stiftung Universitätsmedizin
880 Essen.

881 S.P. was supported by a grant from the Federal Ministry of Education and Research (BMBF)
882 under grant agreement no. 01KI2058.

883 K.Sch. was supported by the German Network for Bioinformatics Infrastructure (de.NBI), a
884 project of the German Federal Ministry of Education and Research (BMBF) [FKZ 031 A
885 534A]. M.E. works within the research building Center for Protein Diagnostics (PRODI),
886 funded by North Rhine-Westphalia state and German Federal funds.
887 L.B. and S.L. received funding from the BMBF (grant no. 01KI20218, CoIMMUNE), the
888 Netzwerk Universitäts Medizin COVID-19 (NUM-COVID-19) within the Network Organo-
889 Strat (grant no.01KX2021), the fund “Innovative Medical Research of the University Muenster
890 Medical School” (grant no. BR111905; to L.B.) and from the German Research Foundation
891 (DFG) for TP6 as part of the CRU 342 (to L.B. and S.L.) and DFG Grants SFB1009 B13 (to
892 SL).

893 Extended Data Figures and legends



894

895 **Extended Data Fig. 1: Treatment with IFN α subtypes reveals distinct antiviral effects**

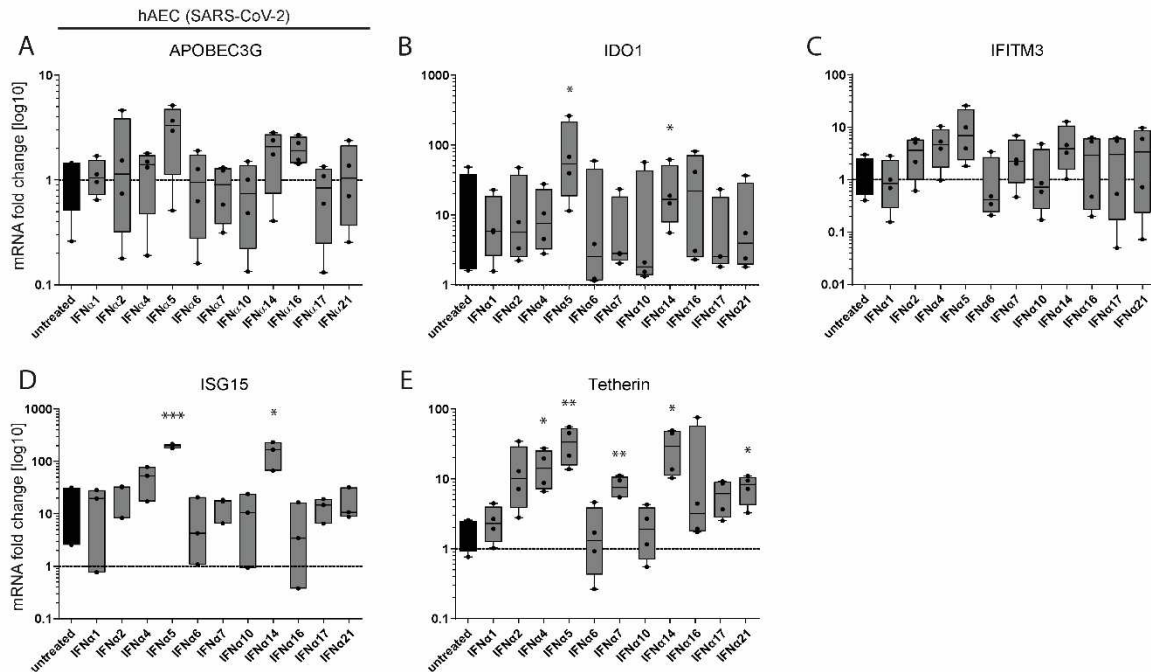
896 **against SARS-CoV-2**

897 (A) Antiviral activity of IFN α subtypes and IFN λ 3 against SARS-CoV-2 were analysed in
 898 VeroE6 cells and cell supernatant by qRT-PCR. IFN α subtypes were titrated against SARS-
 899 CoV-2 on VeroE6 cells by ic-ELISA assay and the IFNs were grouped as mean values in high
 900 (B), medium (C) and low (D) antiviral pattern.

901 Antiviral activity of IFN α subtypes and IFN λ 3 in SARS-CoV-2-infected primary hAECs at 72
 902 h.p.i. determined by qRT-PCR analysis of *M gene* (E) and *N gene* (F). Kinetics of the antiviral

903 activity of IFNs by TCID₅₀ assay grouped into high (G), medium (H) and low (I) antiviral
904 pattern and the mean values of each group are plotted in (J). Mean values of high (I) and low/not
905 (J) antiviral IFNs are shown. Mean values \pm SEM are shown. (A-D) n=3 (E-J) n=4.
906 A: RNA copies /50ng: * p=0.0228 (1000U/mL IFN α 4); * p=0.0110 (1000U/mL IFN α 21); **
907 p=0.0021 (1000U/mL IFN α 5); *** p=0.0008 (1000U/mL IFN α 14); RNA copies/5 μ l : *
908 p=0.0106 (100U/mL IFN α 14); ** p=0.0050 (100U/mL IFN α 5); ** p=0.0017 (1000ng/mL
909 IFN λ 3); *** p=0.0002 (1000U/mL IFN α 4); **** p<0.0001 (1000U/mL IFN α 5, α 14)
910 E: 100 U/mL (ng/mL): **** p<0.0001 (IFN α 5, λ 3); 1000 U/mL (ng/mL): * p=0.0184
911 (IFN α 14); *** p=0.0003 (IFN α 4) **** p<0.0001 (IFN α 5, λ 3); F: 100 U/mL (ng/mL): *
912 p=0.0289 (IFN α 2); ** p=0.0032 (IFN α 4) **** p<0.0001 (IFN α 5, λ 3); 1000 U/mL (ng/mL): **
913 p=0.0019 (IFN α 14); **** p<0.0001 (IFN α 4, α 5, λ 3);
914 G: 48h: * p= 0.0120 (IFN α 2); *** p= 0.0001 (IFN α 4); *** p= 0.0002 (IFN α 14); **** p<0.0001
915 (IFN α 5, λ 3); 72h: ** p= 0.0034 (IFN α 2); **** p<0.0001 (IFN α 4, α 5, α 14, λ 3)
916 H: 48h: * p= 0.0278 (IFN α 7); * p= 0.0179 (IFN α 21); 72h: ** p= 0.0011 (IFN α 7); ** p= 0.0031
917 (IFN α 17); ** p= 0.0037 (IFN α 21)

918



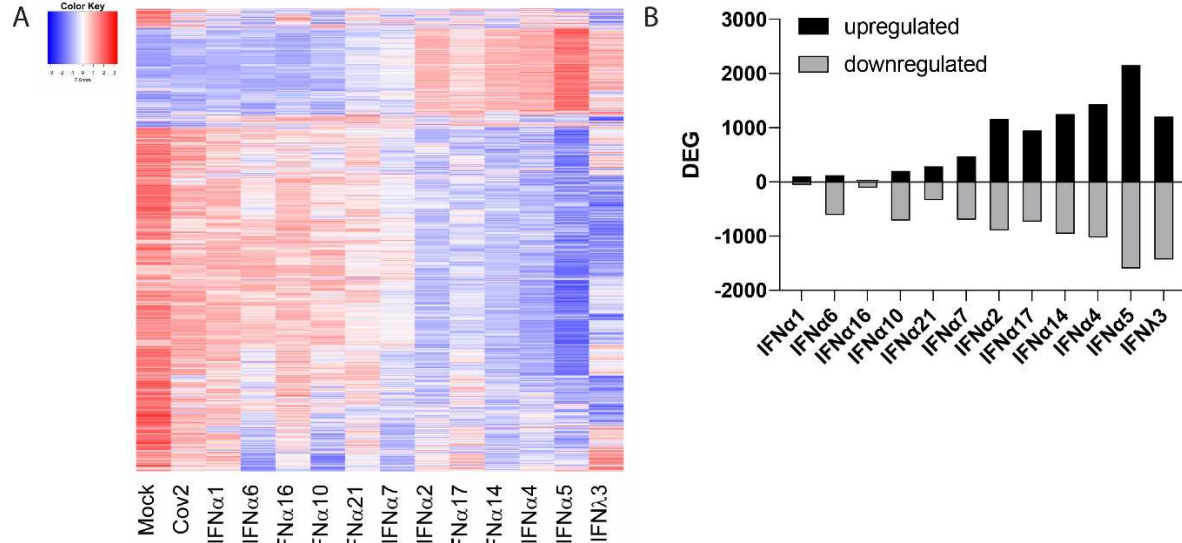
919

920 **Extended Data. Fig. 2: ISG induction upon IFN α subtype stimulation**

921 (A-E) mRNA expression of different ISGs in IFN-treated SARS-CoV-2-infected primary
922 hAECs at 72 h p.i. determined by qRT-PCR analysis. Mean values of mRNA expression is
923 shown as fold change compared to untreated control. (A-E) n=4. B: * p=0.0392 (IFN α 5); *
924 p=0.0460 (IFN α 14); C: * p=0.0198 (IFN α 14); *** p=0.0004 (IFN α 5); D: * p=0.0200 (IFN α 4);
925 * p=0.0197 (IFN α 14); * p=0.0247 (IFN α 21); ** p=0.0087 (IFN α 5); ** p=0.0079 (IFN α 7)

926

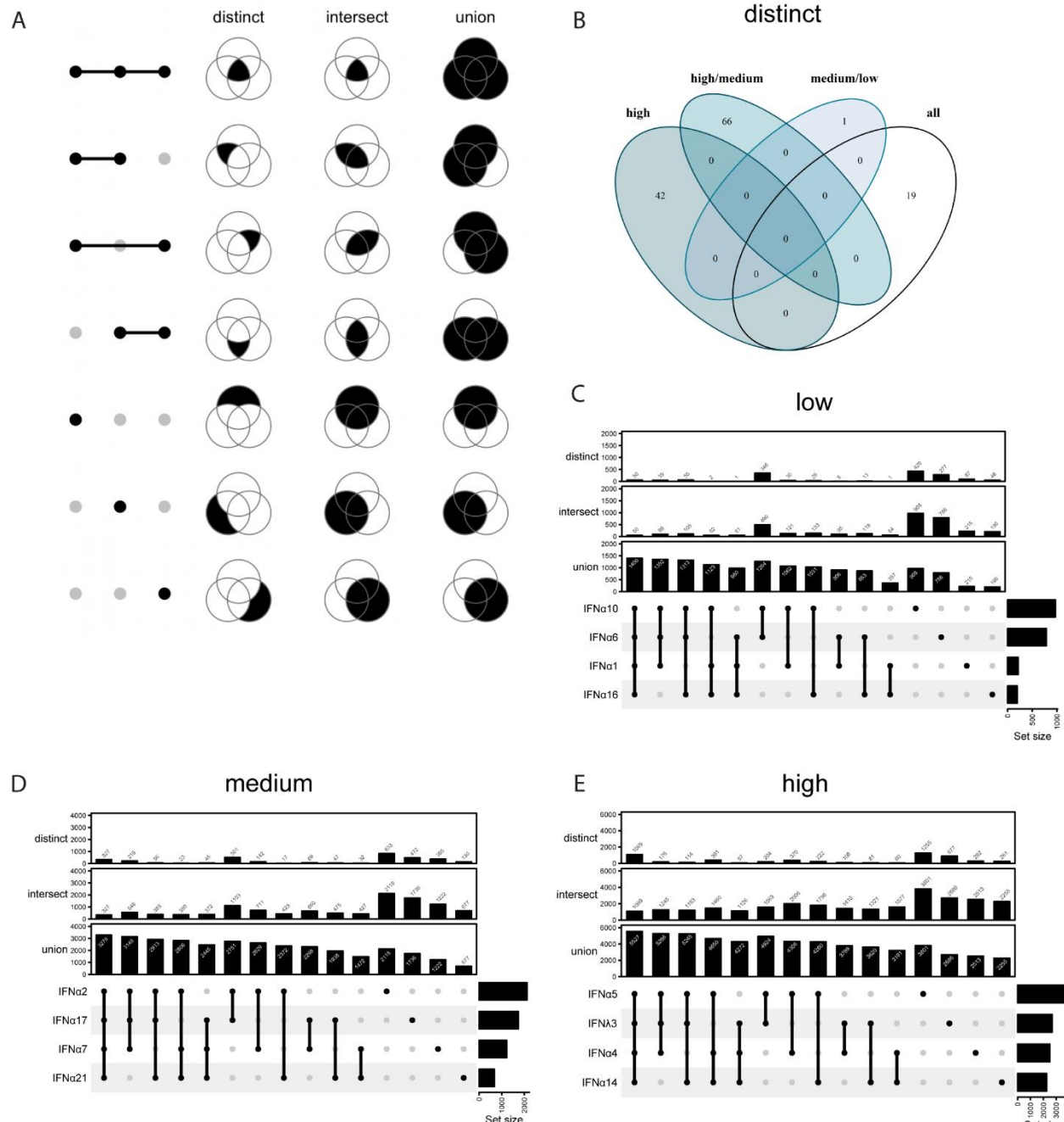
927



928

929 **Extended Data Fig. 3: Transcriptomic analysis display IFN α subtype specific gene
930 signatures**

931 (A) Numbers of up- and downregulated DEGs of IFN-treated compared to untreated hAECs (4
932 donors) shown as bars. (B) Transcriptomic analyses of IFN-treated (16 hours post treatment) or
933 SARS-CoV-2-infected (18 hours post infection) hAECs. Heat maps displaying differentially
934 expressed genes (DEG) from at least one comparison of an IFN vs. Mock.



935

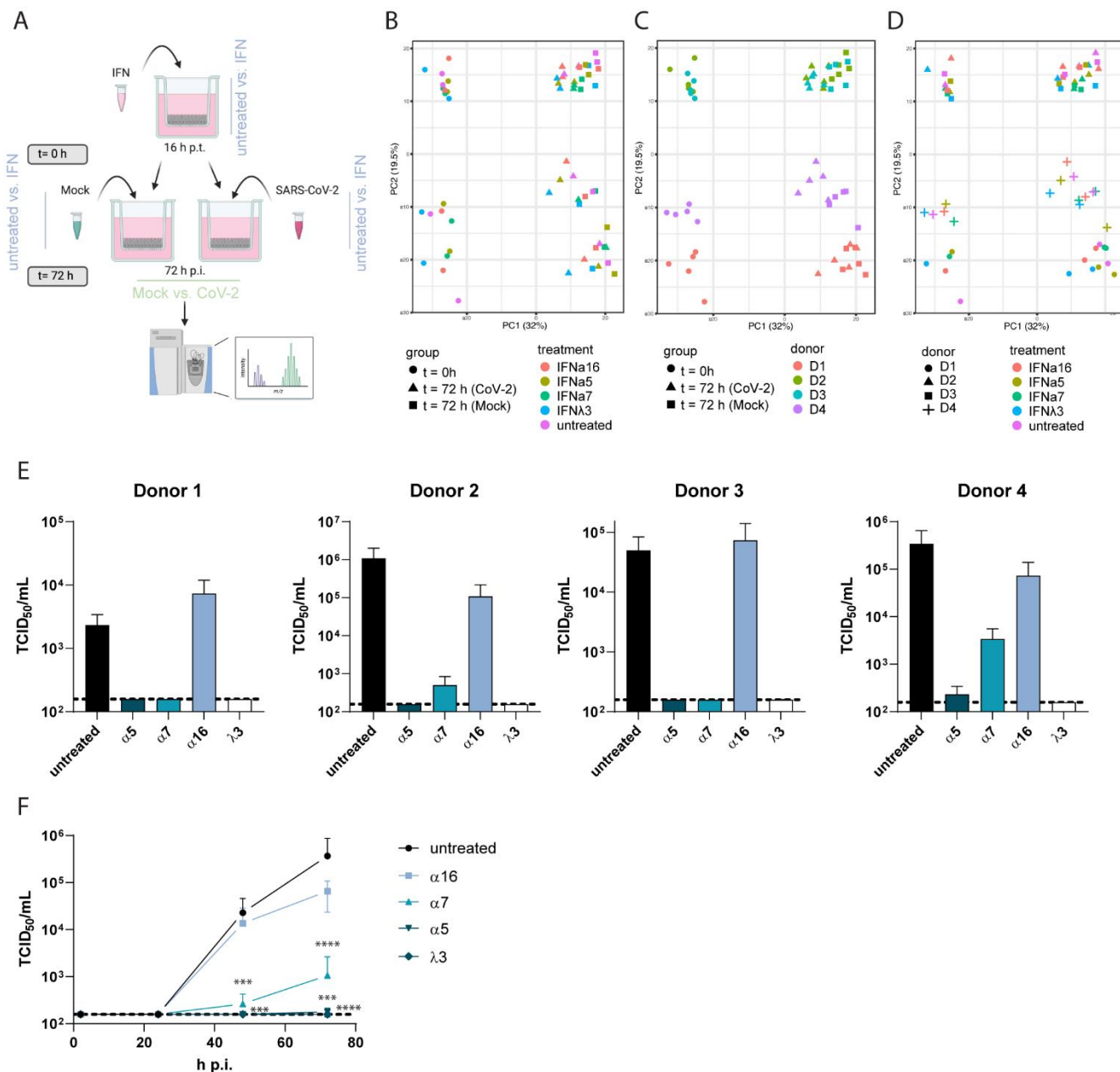
936 **Extended Data Fig. 4: Transcriptomic analysis reveal different patterns of distinct,**
 937 **intersect and union genes**

938 (A-E) UpSet plots to summarize distinct, intersect and union differentially expressed genes
 939 (DEG) of IFN-treated (16 hours post treatment) hAECs (4 donors). (A) Schematic depiction of
 940 distinct, intersect and union DEGs. (B) Venn diagram of distinct DEGs expressed by all high,
 941 medium and low antiviral IFNs. (C) UpSet plots showing distinct, intersect and union DEGs of
 942 low (C), medium (D) and high (E) antiviral IFNs. Numbers of individually or group-specific

943 DEGs are shown as bars and numbers. The bottom right horizontal bar graph labelled Set Size

944 shows the total number of DEGs per treatment.

945



946 **947 Extended Data Fig. 5: Proteomic analysis highlights key cellular mediators**

948 (A-D) Proteomic analysis of IFN-treated and/or SARS-CoV-2-infected hAECs. (A) Schematic
 949 depiction (B-D) Principal component analysis (PCA) of hAEC proteomics. (B) The first two
 950 principal components (PCs) are plotted and shaped/coloured according to group and IFN-
 951 treatment (B); to group and individual donors (C) or to individual donors and IFN-treatment
 952 (D). PCA was performed using all proteins without missing values. Percentage of variation
 953 accounted for by each principal component is shown in brackets with the axis label. (E)
 954 Antiviral activity of IFN α subtypes and IFN λ 3 in SARS-CoV-2-infected primary hAECs of 4

955 individual donors used for proteomic analysis at 72 h p.i. determined by TCID₅₀ assay. (F)

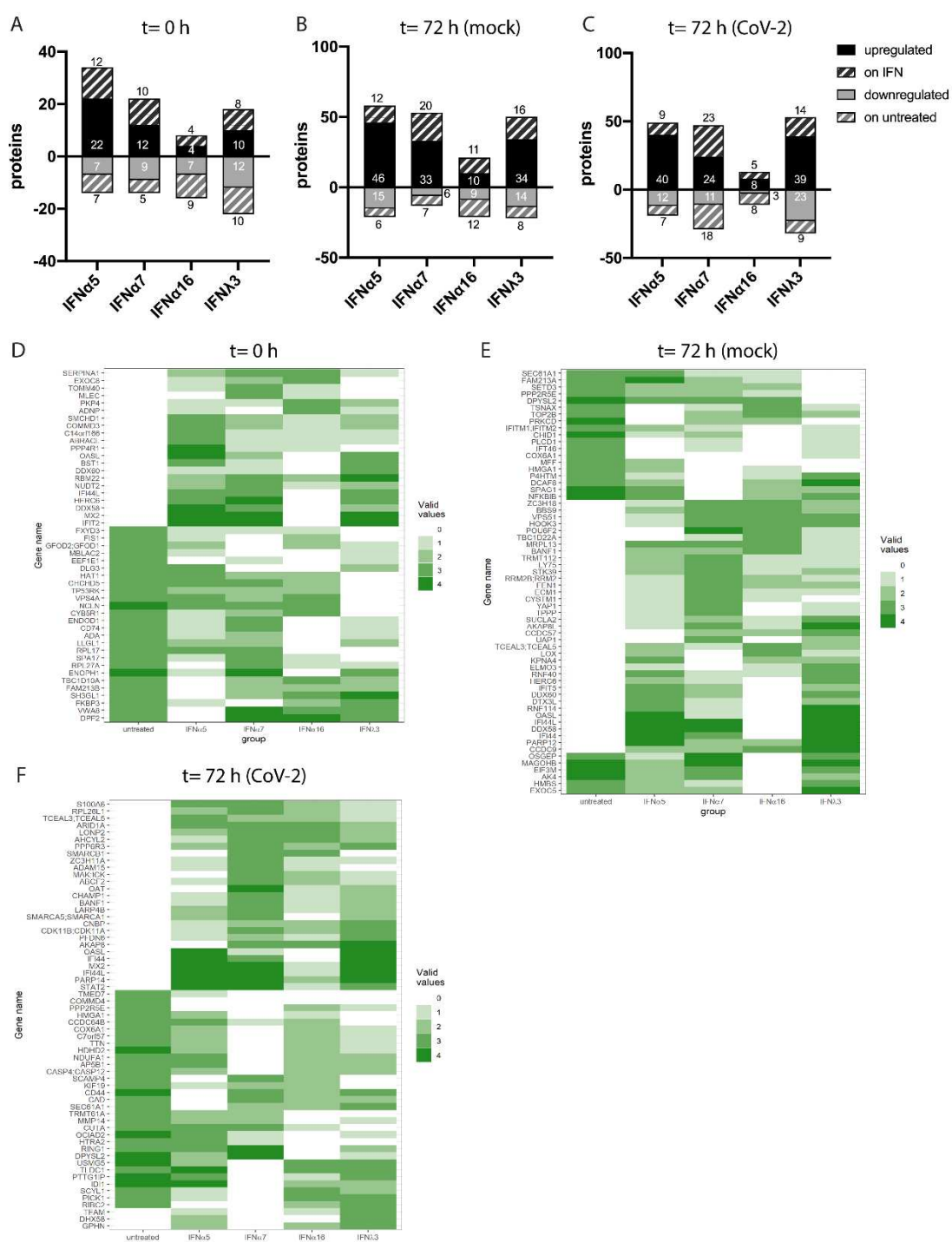
956 Kinetics of the antiviral activity of selected IFNs by TCID₅₀ assay in SARS-CoV-2-infected

957 primary hAECs of 4 individual donors used for proteomic analysis shown as mean values +

958 SEM. D: 48h: *** p= 0.0003 (IFN α 7); *** p= 0.0001 (IFN λ 3, IFN α 5); 72h: *** p= 0.0001

959 (IFN α 5); *** p= 0.0006 (IFN α 7); **** p<0.0001 (IFN λ 3)

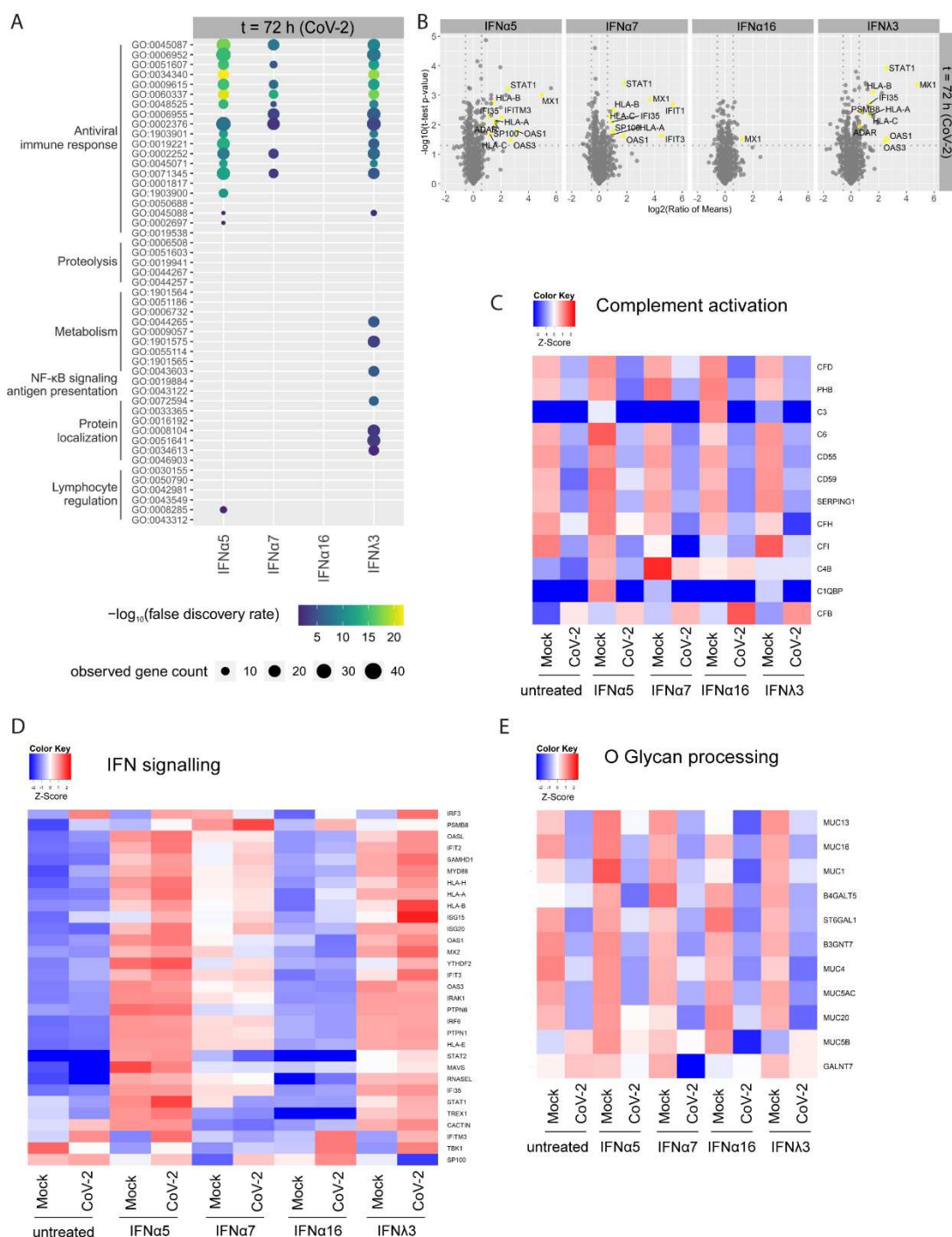
960



961

962 **Extended Data Fig. 6: Proteomic analysis results in differential switched on/off proteins**

963 Proteomic analysis of IFN-treated and/or SARS-CoV-2-infected hAECs. (A) Differentially
 964 regulated or induced (on IFN compared to untreated) proteins in IFN-stimulated hAECs at *t*=0h
 965 (A), at *t*=72h (mock) (B) or at *t*=72h (CoV-2) (C). Heatmaps of on-off regulated proteins in
 966 IFN-stimulated hAECs at *t*=0 h (D), at *t*=72 h (mock) (E) or at *t*=72 h (CoV-2) (F).



967

968 **Extended Data Fig. 7: IFN signature did not change upon SARS-CoV-2 infection**

969 (A-E) Proteomic analysis of IFN-treated and/or SARS-CoV-2-infected hAECs. (A) Biological
970 processes induced by IFNs in SARS-CoV-2-infected hAECs at 88 h p. treatment (t=72 h (CoV-
971 2)). (B) Volcano plots of IFN-treated SARS-CoV-2-infected hAECs (t=72 h (CoV-2)) Detected

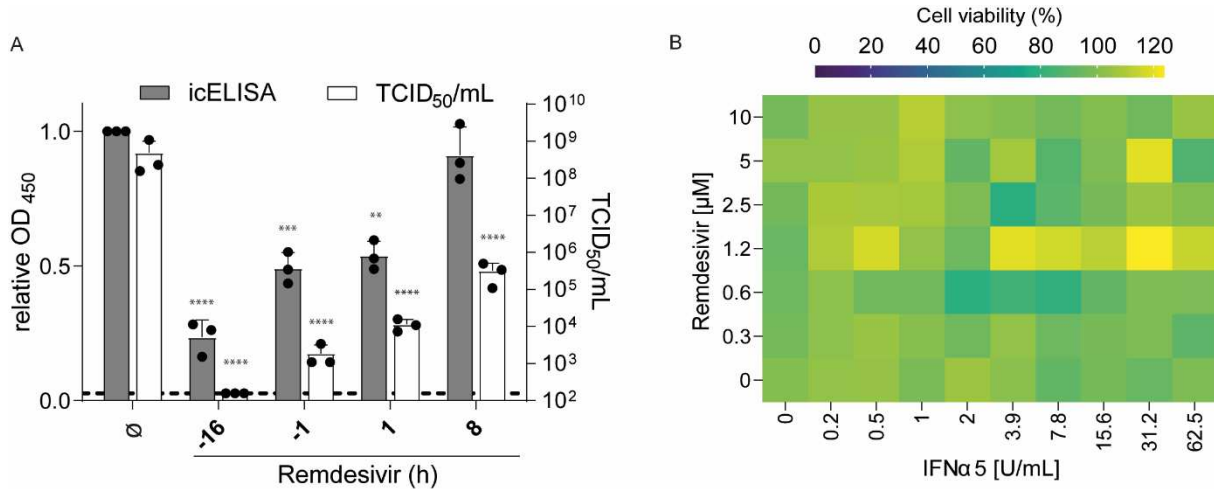
972 ISGs are coloured yellow. Heatmaps displaying differentially expressed proteins which are

973 associated with complement activation (C) IFN signalling (D) and O glycan processing (E).

974 Comparisons of IFN-treated mock or SARS-CoV-2 infected hAECs at 72 h p.i. are depicted.

975 n=4.

976



Extended Data Fig. 8: Therapeutic potential of combination treatment

(A) Pre- and post-treatments of VeroE6 cells with remdesivir analysed by icELISA (black bars) and TCID₅₀ assay (white bars) shown as mean values + SEM. (B) Single and combined pre-treatments of IFN α 5 and remdesivir in SARS-CoV-2 infected VeroE6 cells. Cell viability (%) normalised to untreated control (100%) is shown as heatmap. n=3.

B: icELISA (grey bars) ** p=0.0024 (+1); *** p=0.0009 (-1); **** p<0.0001 (-16); TCID₅₀/mL (white bars) **** p<0.0001 (-16, -1, +1, +8)